Analysis of a LIDAR System at the Harvest Platform for use in Sea-Water Level Measurement and Satellite Altimeter Calibration

by

Scott A Washburn

B.S., University of Colorado, Boulder, 2001

A thesis submitted to the

Faculty of the Graduate School of the

University of Colorado in partial fulfillment

of the requirement for the degree of

Master of Science

Department of Aerospace Engineering Sciences

2011

This thesis entitled:
Analysis of a LIDAR System at the Harvest Platform for use in
Sea-Water Level Measurement and Satellite Altimeter Calibration
written by Scott A Washburn
has been approved for the Department of Aerospace Engineering Sciences

_____
Prof. George Born

_____
Prof. Robert Leben

_____
Dr. Charles Fowler

Date_____

The final copy of this thesis has been examined by the signatories, and we find that both the content and the form meet acceptable presentation standards of scholarly work in the above mentioned discipline.

Washburn, Scott A. (M.S., Aerospace Engineering Sciences)

Analysis of a LIDAR System at the Harvest Platform for use in Sea-Water Level Measurement and Satellite Altimeter Calibration

Thesis directed by Prof. George Born

In July 2007, a new Light Detection And Ranging (LIDAR)-based water-level measurement system was installed at the Harvest platform with the goals of assessing potential drifts in the primary National Oceanic and Atmospheric Administration (NOAA) water level (bubbler) system, and of providing insight on other environmental conditions which may affect the bubbler accuracy. Additionally, the LIDAR provides an independent measure of significant wave height (SWH), which has traditionally been derived from nearby buoys. The open ocean environment of the Harvest Platform has presented significant challenges. Despite these difficult operating conditions, the LIDAR system has shown promise in being able to assess drift in the bubbler as well as the dependencies on SWH and wind speed. However, a longer time series of data, better environmental condition measurements, and better characterization of the laser performance are needed in order to make an assessment of these parameters with the desired accuracy.

Acknowledgements

I am deeply indebted to Dr. George Born, Dr. Bruce Haines, and Dr. Charles Fowler who were all crucial in this work. Thank you for your time, guidance, and most importantly… patience. Thank you to Dr. Robert Leben for sitting on my thesis defense committee. Finally, an extra thank you to Dr. Born for giving me this opportunity and taking a chance on me.

I am also thankful for the help of Mark Bailey, Steve Gill, Caleb Gostnell, Steve Hudziak, and Bob Heitsenrether at NOAA.

This work has been performed through generous support by a National Defense Science and Engineering Graduate (NDSEG) Fellowship, sponsored by the Army Research Office, as well as funding from the NASA Physical Oceanography Program and the Jet Propulsion Laboratory, California Institute of Technology.

Contents

Chapter

Tables

Table

Figures

Figure

1. Introduction

The Harvest project was originally created in response to the need for a dedicated verification site for the TOPEX/Poseidon satellite. This satellite was launched as part of a joint venture between the US's National Aeronautics and Space Administration (NASA) and the French space agency, Centre National d'Etudes Spatiales (CNES), to measure the topography of the world's oceans. With TOPEX's launch in 1992, the satellite provided the most accurate surface topography to date using a combination of radar altimetry and precision orbit determination. This improved topology has led to a better understanding of ocean circulation, ocean dynamics, heat, mass, nutrient, and salt transport, ocean tides, marine geophysics, and the improved knowledge of the marine geoid and lithospheric and mantle processes as well as the ability to monitor globally rising ocean levels (Zeiger et al., 1995).

Since the launch of TOPEX/Poseidon, these Ocean Surface Topography Missions (OSTMs) have been continued with the successive launches of Jason-1 in 2001, OSTM/Jason-2 on 2008, and the future launch of Jason-3 projected for 2013, each satellite hosting improved sensors, precision, and accuracy. In order to maintain a continuous mapping, these satellites were all launched to include overlapping tandem phases such that the satellites were flying the same trajectory separated by only a short distance. Thus these tandem phases allowed for direct comparison of satellite data output. TOPEX/Poseidon was launched on August 10, 1992 and was decommissioned on January 2006. Jason-1 was launched December 7, 2001, providing five years of tandem flight with TOPEX/Poseidon until 2006, and continues to collect data. OSTM/Jason-2 was launched June 20, 2008 and is also currently on-orbit providing data. OSTM/Jason-2

flew tandem with the Jason-1 spacecraft for approximately six months, from July 2008 until January 2009.

The results of the data are used to produce several different products, each with different latencies and thus precision and validation levels. These products in order of increasing latency and precision are the Operational Geophysical Data Records (OGDrs) which are provided with a 3 hour latency; the Interim Geophysical Data Records (IGDRs) which are provided with a two day latency; and finally the Geophysical Data Records (GDRs) which are provided within six weeks with the highest available precision.

By using precision orbit determination to determine the distance from the satellite to the center of the earth, one may subtract the satellite's altitude as determined by the satellite altimeter to obtain the height of the sea surface relative to the center of the earth. In addition to sea level, wave height and wind speed may be measured based upon the shape and strength, respectively, of the altimeter's return pulse.

In addition to the Harvest platform as a calibration/verification site for the US, the CNES also maintains a calibration/verification site is on the French island of Corsica in the Mediterranean Sea (Bonnefond et al., 2003). These two sites provided the initial data for calibration and verification. Since the inception of the program additional sites have been developed to assist in this crucial process, including: the GAVDOS site on the island of Gavdos, Crete, Greece in the Mediterranean Sea, jointly operated by the European Union (EU), NASA, and the Swiss Federal Government (SFG) (Pavlis et al., 2004); the Ibiza site on the Spanish island of Ibiza in the Mediteranean Sea, operated by the Spanish Space Program with assistance from CNES and NASA (Martinez-Benjamin

et al., 2004); an additional US NASA site on Lake Erie (Shum et al., 2003); and the Bass Strait site off the island of Tasmania, Australia, operated by the Centre for Spatial Information Science at the University of Tasmania (Watson et al., 2003). Each site utilizes slightly different methodologies in their calibration/validation approach and each has its own unique advantages and disadvantages.

2. The Harvest Platform

The Plains Exploration and Production (PXP) Harvest Oil Platform (Figure 1) is located about 10 km off the coast of central California near Vandenberg Air Force Base. In addition to its primary function to drill for oil in the Santa Maria Basin, Harvest has served as a calibration site for the joint U.S./France TOPEX/POSEIDON (T/P, 1992–2002), Jason-1 (2001–2009) and Ocean Surface Topography (OSTM/Jason-2, 2008–pr.) missions (Haines et al., 2010). The 30,000-ton platform is anchored to the sea floor and sits in about 200 m of water near the western entrance to the Santa Barbara Channel (Figures 2 and 3). Conditions at Harvest are typical of the open ocean: ocean swell and wind waves average 2–3 m, though waves over 7 m have been experienced during powerful winter storms. Prevailing winds are from the northwest and average about 6 m/s.

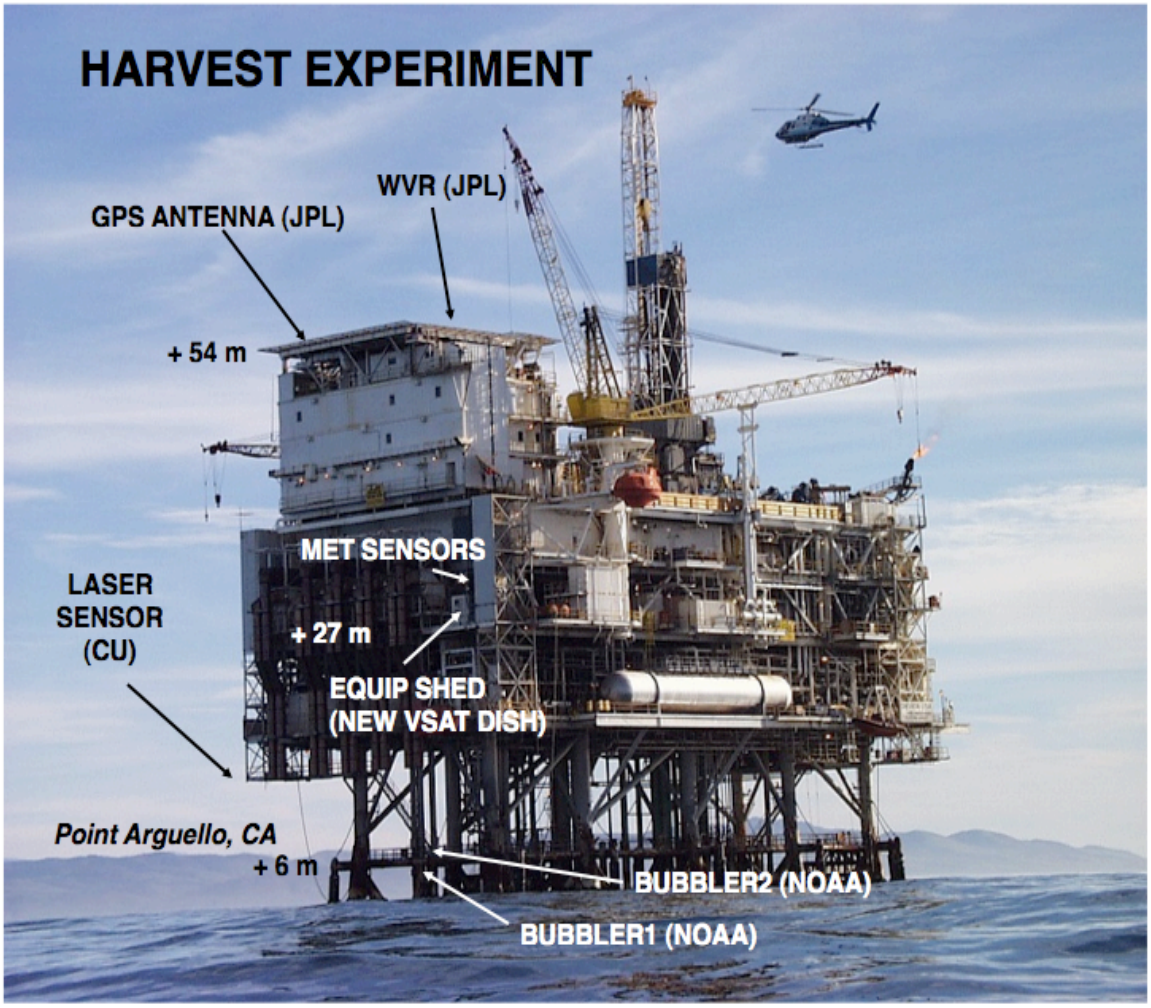

Figure 1: Photo of *PXP* Harvest Platform. The platform sits in 200 m of water, and extends approximately 50 m (excluding derrick) above the mean water level.

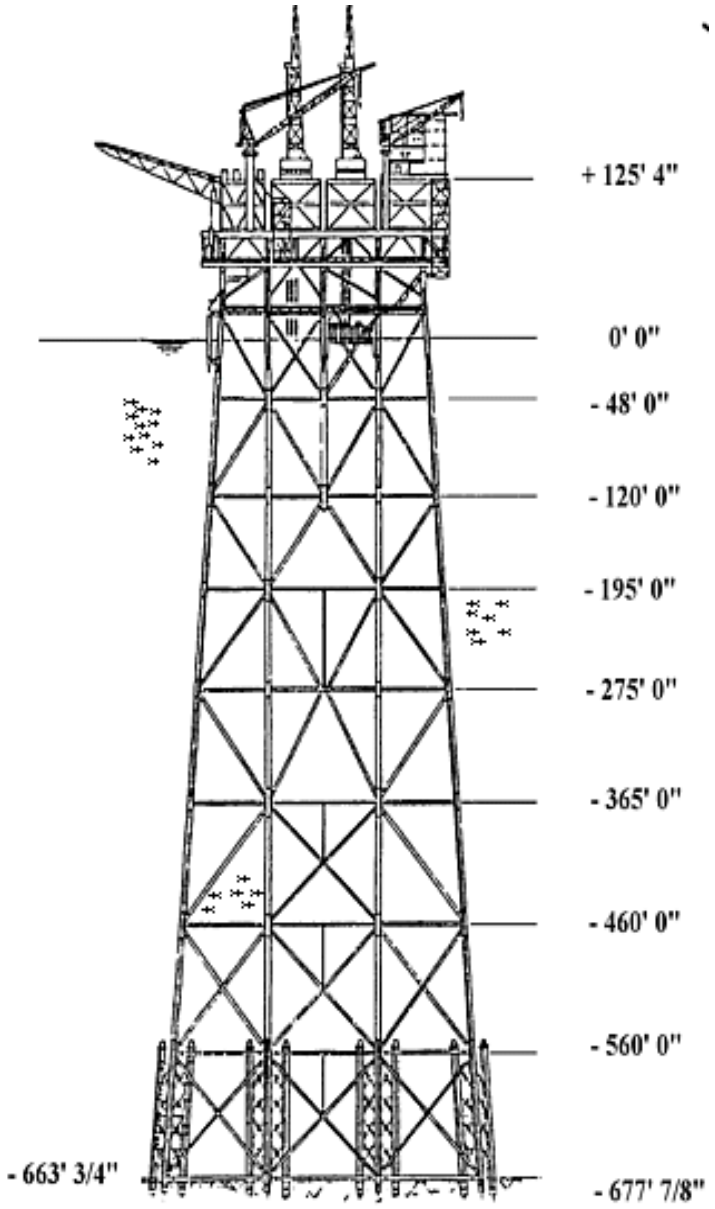

Figure 2: Side profile of the Harvest platform, including the submerged structure.

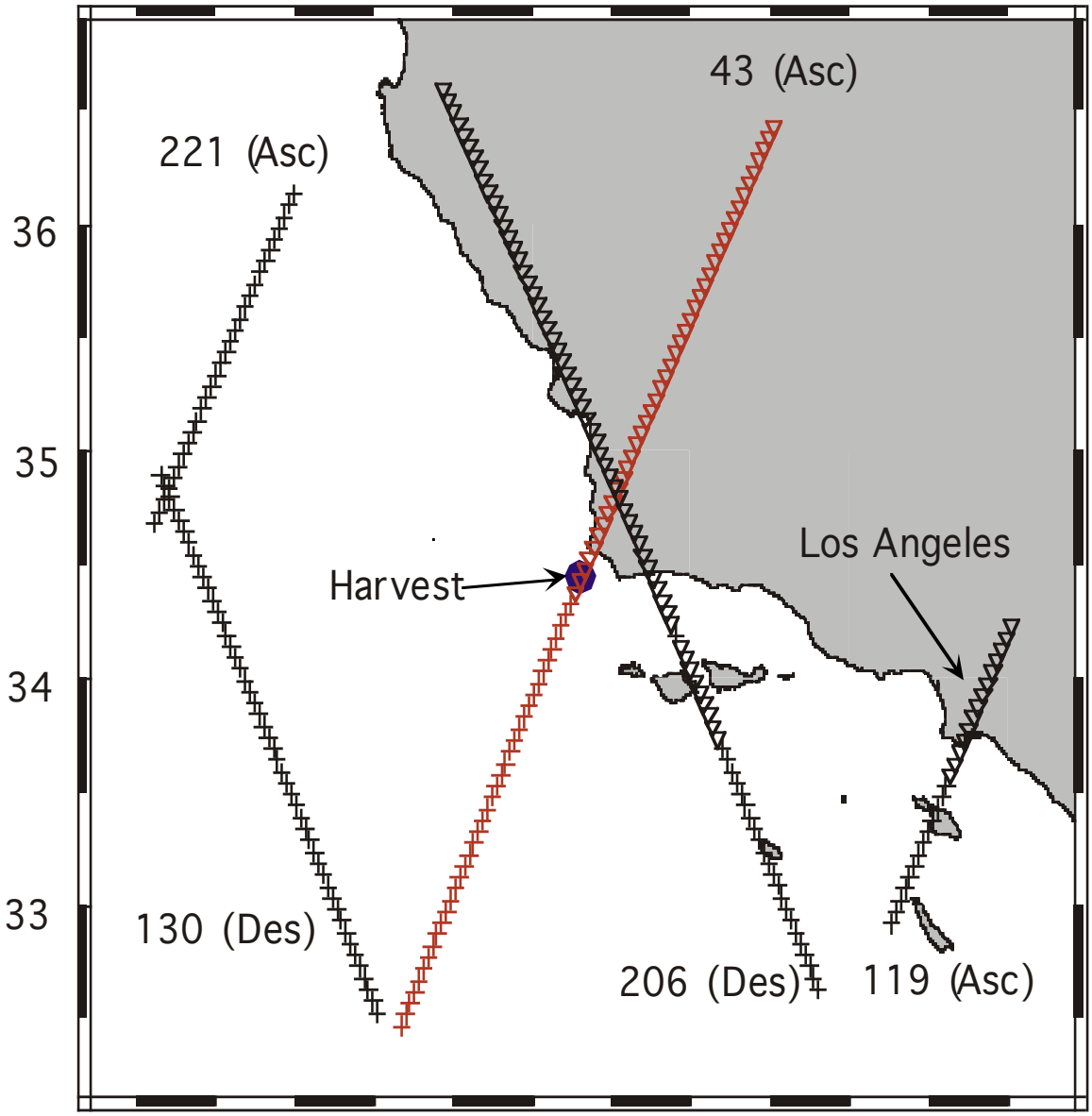

Figure 3: Satellite overflight ground tracks at Harvest platform.

The Harvest experiment features carefully designed collocations of space-geodetic and tide-gauge systems to support the absolute calibration of the altimetric sea-surface height (Haines et al., 2010). The bias and stability of the sea-surface height (SSH) are important elements of the altimeter system error budget (Chelton et al., 2001; Bonnefond et al., 2010). Knowledge of this bias is essential for

specialized studies that rely on accurate determination of scale, such as determination of the Earth's mean radius. More important, estimates of the biases are needed to merge data from different missions, or from different measurement systems on the same mission, in order to calibrate altimetric time series of global mean sea level (Haines et al., 2010).

The SSH calibration for these satellites is performed using measurements from the primary National Oceanic and Atmospheric Administration (NOAA) water level system installed at the Harvest platform (Haines et al., 2010). Since October 2002, the NOAA system has used digital bubbler gauges exclusively. While the NOAA systems are very stable, the Harvest bubbler operates in open-ocean conditions and the measurements exhibit systematic variations stemming from the large variations in sea state. Due to the importance of monitoring the long-term drift of the altimeter SSH, it is important that the stability of the bubbler system is monitored using independent water-level measurements.

In July 2007, a new Light Detection And Ranging (LIDAR)-based water-level measurement system was installed by the University of Colorado at the platform with the goals of assessing the stability of the bubbler system, and of providing insight on other environmental conditions that may affect the bubbler accuracy. Additionally the LIDAR system may prove an eventual successor to the traditional submerged tide gauges as it provides a number of distinct advantages including ease of maintenance (notably the lack of any underwater maintenance), low cost, and ease of remote operation and reconfiguration. The laser unit itself is relatively inexpensive compared to radar and acoustic systems currently in use and costs approximately $2250, while a commercial system such as the MIROS SM-094/2 Range Finder (a microwave device) costs over

$20,000. The only maintenance currently performed is periodic cleaning of the laser view-window to remove deposits from the atmosphere and sea spray.

3. Bubbler System

Bubbler tide gauges operate by forcing pressurized air at a metered rate through a small-bore tube to a pressure point which is fixed underwater, below the lowest expected sea level. The pressure point is normally a short vertical cylinder which is closed at the top where the metered air enters the chamber and open at the bottom. A small "bleed hole" is drilled about halfway down the cylinder. As metered air from the tube enters the cylinder, it becomes compressed and pushed the water down inside the cylinder until the level of the bleed hole is reached, at which point the air starts to bubble out and back towards the surface. This is shown below in Figure 4. As long as the air flow rate is low and the air supply tube is not too long, the pressure of air in the system will equal that of the pressure due to the depth of the sea water above the bleed hole coupled with atmospheric pressure (IOC Vol IV, 2006). Water level is then recorded as a function of the equation:

$$h = (p - p_a)/(\rho g) \qquad \textbf{Eq. 1}$$

Where:

h = height of sea level above the bleed hole

p = measured pressure

p_a = atmospheric pressure

ρ = seawater density

g = gravitational acceleration

Prior to the launch of T/P in 1992, NOAA personnel installed a Next Generation Water Level Measurement System (NGWLMS) at the Harvest Platform on risers serviced from the 20-ft boat-landing deck. This system originally consisted of a self-calibrating acoustic sensor and a secondary digital "bubbler" (Gill et al., 1995; IOC, 2006). In support of the Jason-1 mission, NOAA personnel replaced the NGWLMS with an updated system. The acoustic system—inoperative after storm damage in May 1999—was converted to a bubbler in October 2002, and the original bubbler was refurbished in April 2003. There were several reasons for changing to an all bubbler system, one of them being that the conditions at Harvest are outside of the optimal performance range of the acoustic system. Each measurement system is now identical, one serving as the primary sensor, the other as a redundant, although each may be used interchangeably.

Along with the acoustic sensors, Paroscientific sensors in the digital bubbler configuration are now used as primary sensors in the NOAA network where acoustic sensors cannot be installed. Using Paroscientific pressure transducers with internal temperature compensation technology, vented to the atmosphere and located out of the water, the potential loads that can cause drift are minimized. Both digital bubblers on Platform Harvest are equipped with a Paroscientific sensor in this configuration. Currently no sensor drift has been found in any of these systems. Additionally, the systems are checked and leveled as part of annual maintenance and the two sensors are compared monthly as part of NOAA's regular quality control with no noticeable drift between the two sensors (S. Gill, personal communication, February 17, 2011).

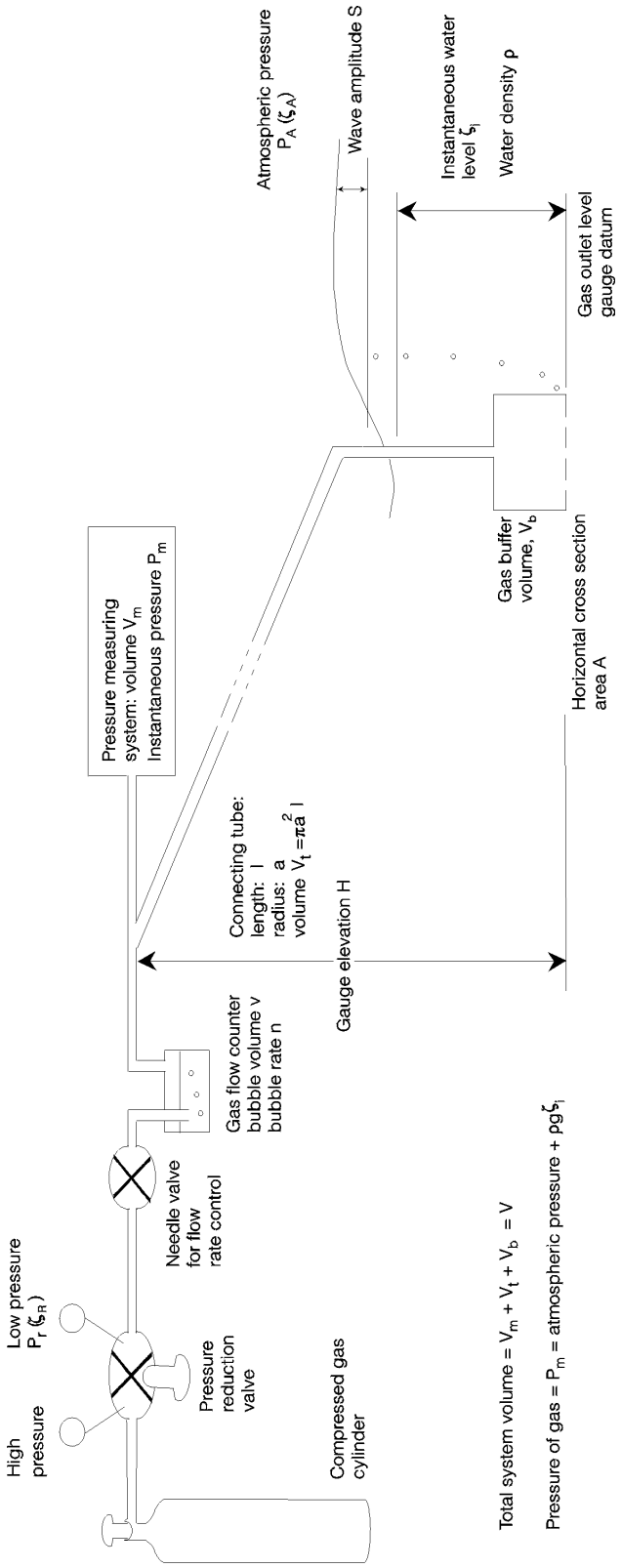

Figure 4: Schematic of a Bubbler Pressure Gauge System (IOC Vol III, 2002).

Bubbler water level measurements are recorded every 6 minutes, based on a 3-minute average of 1 Hz observations (181 measurements) centered on the reported interval. This data is transmitted via GOES satellite after which it is made available on the NOAA Tides and Currents web site[1]. Raw (Unprocessed) "Preliminary" water level data are available in near real time. NOAA performs additional post-processing on these data, making them available in "Verified" form approximately one month later. The raw Preliminary data are used in the satellite altimeter closure analysis (the combination of all available data resulting in a final SSH value for the Geophysical Data Record (GDR)) and are used for the analysis presented in this paper as well. The use of the "Preliminary" data instead of the "Verified" data is primarily due to the fact that some of the bubbler post-processing performed by NOAA appears inconsistent over the time-series analyzed.

4. LIDAR System

In July 2007, the University of Colorado installed a new LIDAR-based water-level measurement system on the 47-ft sump deck of the platform. This LIDAR system consists of a downward-looking laser sensor, protected by a cast aluminum enclosure with a glass bottom view-window, as shown in Figure 5. Data is transmitted via ethernet cable to a laptop in the Jet Propulsion Laboratory (JPL) equipment shed at the 87-foot level. Raw measurements are stored in the laptop until downloaded via a satellite internet connection.

[1] http://tidesandcurrents.noaa.gov/geo.shtml?location=9411406

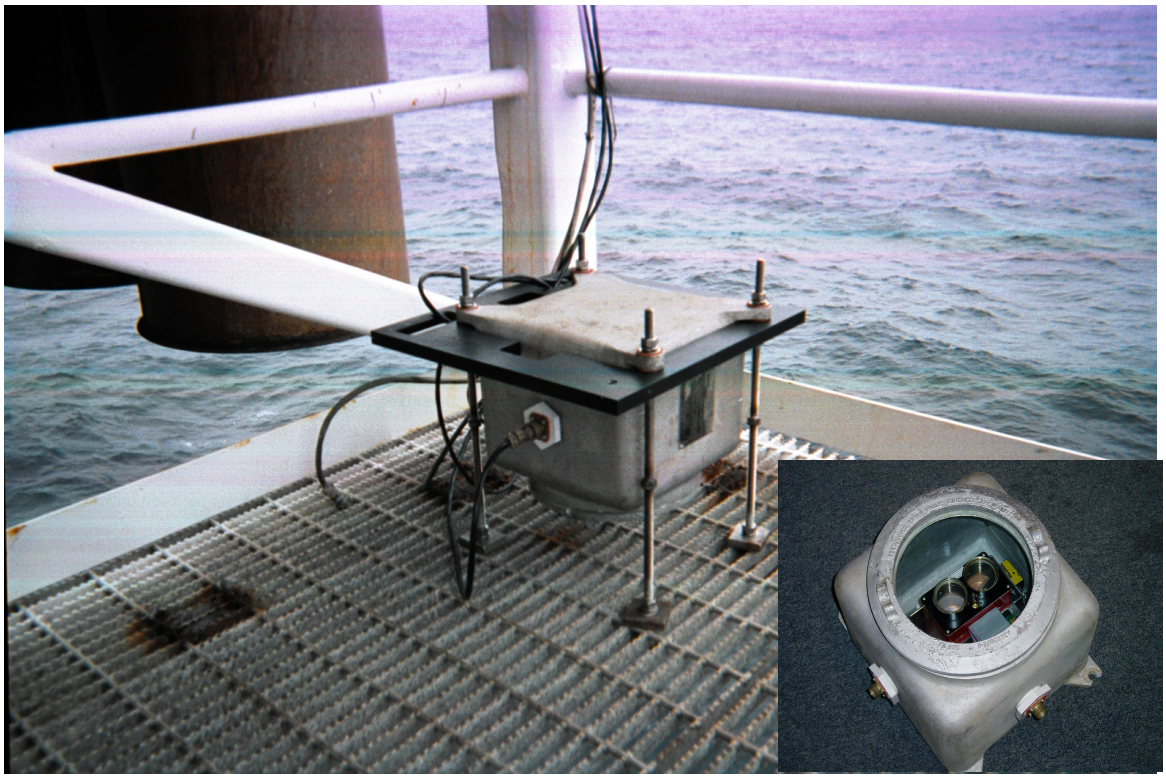

Figure 5: Photo of LIDAR enclosure onboard the *PXP* Harvest Platform. Inset shows bottom view of enclosure with laser unit visible.

The Harvest laser is a Laser Technology Inc. Universal Laser Sensor (ULS)[2], which has a variety of operating modes available for different applications and has a Pulse Repetition Frequency (PRF) range from 1 – 4000 Hz. The ULS laser was selected over other water level measurement systems primarily for its low cost and availability. The same ULS laser has been successfully tested by NOAA for use in bridge-gap measurement systems (NOAA 2010) but has not to our knowledge been used in an open-ocean environment with such extreme operating conditions. With significant wave height (SWH) regularly reaching values of 5 m or more and wind speeds in excess of 15 m/s, the harsh environment at Harvest resulted in lower than expected performance of the laser. However, despite these difficult operating conditions, the LIDAR system has shown

[2] http://www.lasertech.com/

promise in being able to assess drift in the bubbler as well as the dependencies on SWH and wind speed. It is important to note that despite the fact that the ULS laser has been successfully used by NOAA for bridge-gap measurements, this environment is extremely benign. Additionally, the operational requirements are significantly lower than required for purposes of the Harvest project. After speaking with Bob Heitsenrether at NOAA who was responsible for some of the testing done on the ULS system for NOAA, they experienced many of the same problems and issues with the laser described later in this paper. For certain applications NOAA deemed these acceptable.

The University of Colorado had maintained a LIDAR system at the Harvest platform prior to the installation of the system used for this analysis. Unfortunately there are no records of this system's setup or data to utilize for comparison.

4.1. Laser

The ULS's integrated laser processing allows the specification of a pulse-per-measurement (PPM) count in addition to the PRF. Together, the PPM and PRF dictate the laser output measurement rate. Several laser parameterization schemes were utilized, but all configurations were selected to maintain a 50 Hz measurement output rate from the laser. This 50 Hz output was maintained simply for ease of use. Changing the laser output rate would have required changing of the laser processing code and did not seem prudent or necessary. In addition, the integrated laser processing allows the selection of several different modes of laser processing. The two employed in this experiment were "Last Targeting" and "Averaging." Last Targeting (LT) mode records the longest return in a specified interval, and is the manufacturer's recommended mode in open-ocean

environments where factors such as sea spray and foam can result in measurements that are erroneously short. Averaging (AV), as the name implies, is simply the average of laser measurements over a specified time period.

It is also important to note that Averaging mode also employs an additional setting termed Average Weight (AW) or Minimum Good Pulses. This setting defines the minimum number of good pulse returns which must be obtained in a given measurement interval before an average measurement value is taken. Once this minimum value is reached the average is calculated using these returns. Thus if AW is set to 10, as soon as 10 good pulses are obtained the average is calculated (i.e. any additional good pulses obtained during the measurement interval are not included in the average, regardless of the PPM value). All Averaging modes discussed in this research utilized an AW of 4. Additionally, the power setting for the laser was maintained at its maximum value (with setting options of Maximum, Medium, or Minimum).

Three different types of laser setting combinations were employed: 1) LT mode with PRF of 500 Hz and PPM of 10; 2) LT mode with PRF of 4000 Hz and PPM of 80; and 3) AV mode with PRF of 500 Hz and PPM of 10. All three settings thus maintained a laser measurement output rate (PRF/PPM) of 50 Hz. Each of the three laser modes was selected to try and characterize the different operating modes and settings of the laser. Unfortunately this proved to be extremely difficult given that this was done remotely without anyone directly observing conditions at the platform. Environmental conditions, as discussed later, are derived from nearby sources and are assumed to be representative of local conditions at the platform over a longer time-series. However, assessing the immediate conditions experienced by the laser is impractical and thus accurate

characterization of the laser modes and settings was not possible. Despite this, each setting displayed no distinguishable difference in the overall laser noise levels, however the different laser settings did result in a significant shift in the laser bias.

Because the laser was not fully tested prior to it's installation at the platform, the performance characteristics of the laser in its various operating modes have not been fully characterized. Ultimately it was decided to leave the ULS in the first mode (LT mode, PRF 500, PPM 10) to maintain consistency and to extend the life of the laser since higher PRF rates can shorten the laser's expected lifetime.

4.2. LIDAR Data Processing

The 50 Hz laser output measurements are processed so that they are comparable to the output of the bubbler system. The 50 Hz returns are averaged to provide 1 Hz measurements which are recorded and stored until retrieved by the user. For each 1 Hz measurement, the following data are recorded: the minimum 50 Hz return, the maximum 50 Hz return, the mean 50 Hz return, and the percentage of good 50 Hz returns (i.e. the percentage of 50 Hz measurements where an actual measurement was obtained as opposed to an error reading from the laser). This last metric is a good indication of laser performance and, as discussed later, is used later for correction of the laser output.

After these 1 Hz data are compiled, they are then filtered and processed to provide SSH measurements using the same method as the bubbler. The 1 Hz data are initially filtered for erroneous readings. The mean 50 Hz laser return typically reads between 11 and 14 meters. Thus any mean 50 Hz laser measurement which is less than 8 m or greater than 20 m is removed. Additionally a filter of 3 m is imposed on the 50 Hz measurement

range (i.e. the maximum 50 Hz return minus the minimum 50 Hz return). Thus a 1 Hz measurement which contains an extreme data point which has significantly offset the mean 1 Hz measurement will be ignored.

The data are then averaged to provide 6-minute SSH measurements using the 181 data points centered on the interval. Thus the 6-minute data output provided by the laser and bubbler reports an average value for the specified period using the identical time interval. In addition to the SSH measurement average, the following data are recorded: 1) the percentage of good 1 Hz returns (i.e. the percentage of the 181 1 Hz measurements where at least one good 50 Hz return from the laser was recorded), which is used for filtering; and 2) the average 50 Hz return percentage, which is the average of the percentage of good 50 Hz returns for the 1 Hz data points being averaged, and is used for regression. These parameters are discussed in greater detail later as they are used for filtering and regression analysis.

5. Sea Conditions and Meteorological Data

Meteorological data used in correcting the bubber and laser data were obtained from several sources. Significant wave height (SWH) data are obtained from the Scripps Institution of Oceanography Coastal Data Information Program (CDIP) Harvest buoy[3], which is located approximately 5 nm west of the platform. The CU LIDAR system also provides an estimate of SWH. Sea-surface temperature, air temperature, atmospheric

[3] http://cdip.ucsd.edu/?sub=data&nav=historic&stn=071&stream=p1

pressure and wind speed are obtained from the NOAA National Data Buoy Center (NDBC) Pt. Arguello buoy[4] located approximately 20 nm northwest of the platform.

Unfortunately, these environmental data provide only an approximation of actual conditions at the platform due to the large separation distances between the data sources and the Harvest platform. However the data do provide a rough scale approximation of the platform conditions and as such are used for the regression analysis described later. Atmospheric pressure and air temperature are also available from the NOAA Tides and Currents website from the same location as the bubbler. When I first started to assess sources for temperature and pressure, the NOAA platform data for these parameters[5] appeared to only be available intermittently and it was decided to use data from the NDBC buoy which was regularly available. However, after looking at the platform source again these data are actually available hourly and since August of 2010 they have been available every six minutes to coincide with the reported bubbler water levels. Future work on this project should try the regression analysis described later utilizing the temperature and pressure data from the platform.

The lack of environmental sensors in the immediate vicinity of the platform presents a significant problem for determining environmental effects on the instruments. As we will see in later sections, the measurement difference between the bubbler and the laser is affected by both wind speed and SWH. While SWH can be assessed using the laser, the only source for wind speed data is located approximately 20 nm away. This data is a poor proxy for local wind speed at the sensor location. Even slight variations in

[4] http://www.ndbc.noaa.gov/station_page.php?station=46023
[5] http://tidesandcurrents.noaa.gov/data_menu.shtml?stn=9411406%20Oil%20Platform%20Harvest,%20CA&type=Meteorological+Observations

wind speed and direction can cause significant changes in ocean surface effects. Given that wind conditions themselves can vary significantly in the ocean environment over distances of several meters, a distance of 20 nm only provides data for regression analysis on a macroscopic scale. This logic similarly applies for other environmental factors such as temperature and pressure.

On recommendation for future improvements in the experiment would be to install local sensors at the platform, ideally in the immediate vicinity of the sensors, in order to obtain a more accurate and locally viable regression (i.e. individual data points vice macro of the time-series).

6. SWH Comparison

SWH, or $H_{1/3}$, is defined as the average of the highest one-third of the waves (as measured from peak to trough) in a given time period. This measurement was originally designed to give a computational estimate of what an observer would visually detect with the naked eye. It is commonly estimated as four times the RMS of the wave time-series (Kinsman, 1965). For calculating the SWH using the LIDAR system, the latter estimation method is used with the same three minutes of data utilized to calculate the average SSH. This is a more common method of calculating SWH, as well as being the method used for the buoy where SWH is traditionally compared, and has values closer to those of the buoy.

SWH estimates between the Scripps Buoy, traditionally used in SWH correction of the bubbler, and the laser derived SWH vary significantly over the three-year period since collection began. Over the available time-series, the difference between the buoy

and laser SWH calculated using the 4-times-rms method has a mean of 0.17 m, a sample standard deviation (σ) of 0.38 m, and is as large as 3.5 m. Given that the sensors are located approximately 5 nm apart, this is not unexpected.

In addition to the SWH data available from the Scripps buoy, the scatter of the bubbler SSH 1 Hz data is available[6]. This 1 Hz scatter can be evaluated as a proxy for SWH (similar to the 4-times-rms method) for use in comparison to the laser derived SWH. Unfortunately the availability of this data was not known by myself until just before the publishing of this thesis and therefore was not able to be analyzed. This would be a valuable comparison for future work.

We may also compare the laser and buoy derived values for SWH with those of the satellite altimeters during flyover times. It should be noted that the satellite derived SWH is based upon the slope of the leading edge of the return signal (Parke and Morris, 1995). This SWH estimate is that of the entire footprint of the altimeter. Based upon typical SWH values this footprint is approximately 3km in diameter, but increases to as much as 7 km in diameter with increasing SWH (Parke and Walsh, 1995), and thus could vary substantially from the locally derived value at the platform. Data showing the mean and standard deviation between the altimeter and the laser and buoy sources is shown below in Table 1. Additionally, the SWH from the satellite, laser, and buoy for satellite overflights are shown below in Figures 6 and 7 for visual comparison.

[6] http://opendap.co-ops.nos.noaa.gov/axis/webservices/waterlevelrawsixmin/index.jsp?id=9411406&&d=MLLW

Source	Jason-1 Altimeter Comparison		Jason-2 Altimeter Comparison	
	Mean [m]	Standard Deviation (σ) [m]	Mean [m]	Standard Deviation (σ) [m]
Buoy	-0.1963	0.2559	0.0218	0.7283
Laser	0.0723	0.2132	0.2004	0.7100

Table 1: SWH Comparison

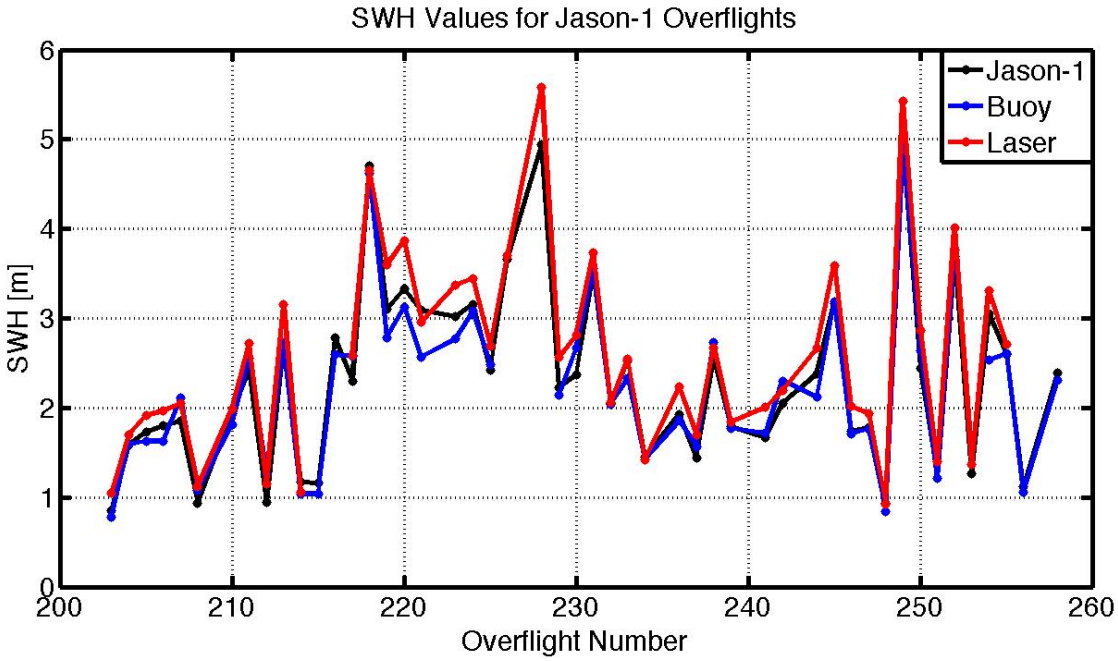

Figure 6: Jason-1 flyover SWH comparison

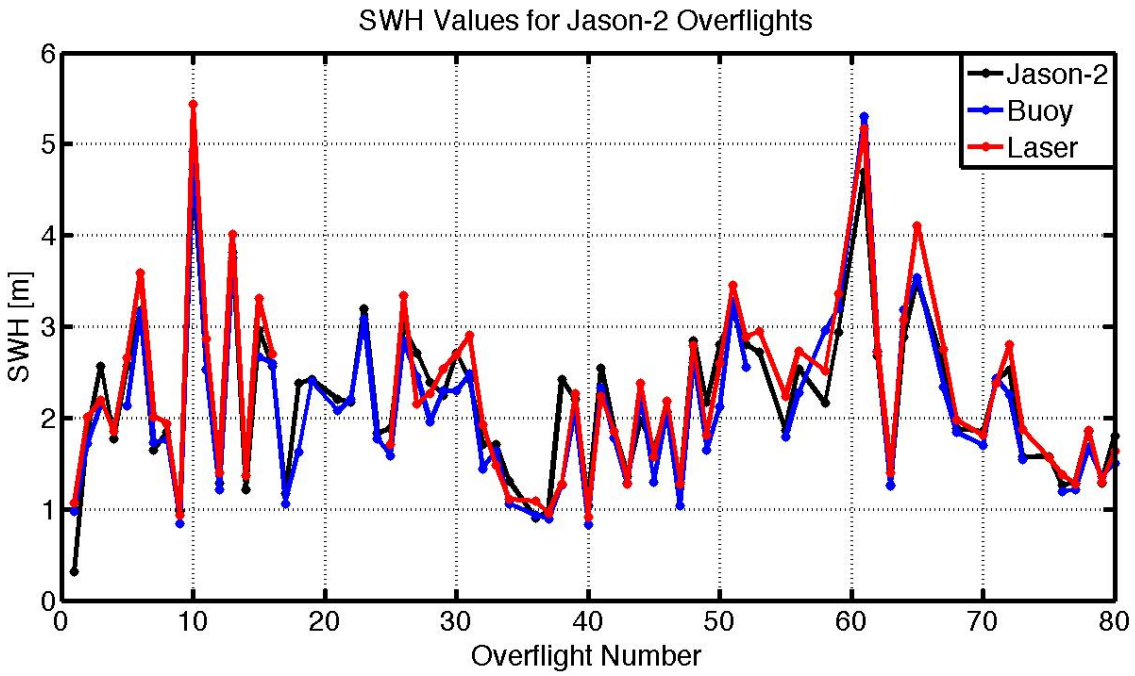

Figure 7: Jason-2 flyover SWH comparison

Subsequent analysis and regressions utilize the laser-derived SWH since this is assumed to be more relevant, given its collocation with the bubbler and flyover paths, and also due to several gaps in the bubbler data (notably due to data acquisition problems in Nov 2007, and the buoy drifting offsite in Dec 2008).

7. Bubbler Laser SSH Measurement Comparison

With the CU LIDAR system in place since July 2007, over three years of simultaneous bubbler and laser data can be compared. No accurate survey of the laser location has been conducted, so the vertical separation of the units must be estimated, but it is known to be approximately 27 m. This vertical separation is estimated as part of the regression analysis discussed later. Additionally, the units are not located directly over

one another, but their horizontal separation is considered negligible since water-level measurements are being compared over an average of 3 minutes worth of 1 Hz data.

7.1. Laser Mode and Bias Correction

When I took over the Harvest project in August of 2009, the laser was operating in the Last Target mode with the PRF at 500 Hz and PPM at 10 (thus giving the 50 Hz laser output as described previously). Unfortunately there were no previous records or logs indicating any changes in the laser settings prior to this date. After talking with Chuck Fowler who was involved with the initial setup of the laser, he believed that the laser had been maintained in this same setup since data recording began in July 2007. I attempted to visually sort through the data and look for any breaks with associated bias shifts. However it turned out to be impossible to positively identify any mode or setting shifts. The remainder of this analysis assumes that the laser was operating in the mode and settings described above during this time

As stated earlier, three different types of laser setting combinations were employed. These different methods were explored to determine if any system performance improvements could be realized. While not displaying any apparent changes in the noise level of the laser measurements, changes in the laser mode settings introduced considerable shifts in the laser bias as shown in Figure 8. These biases were estimated by comparing the bubbler and laser water-level measurements immediately before and after the mode shifts occurred. Due to the relatively close trending of the two measurement systems, the two measurements could be overlayed with one another and the laser bias following the mode shift could be estimated by matching the slope of the

bubbler data. Noise in both the laser and bubbler systems made it difficult to accurately asses these biases, however the error in the bias correction is estimated not to exceed 0.5 cm. Errors in the bias correction could impact the subsequent regression analysis but are assumed negligible for the remainder of this analysis.

When shifting operation of the laser from Last Target mode to Averaging mode the laser readings tended to be closer, thus making the difference between the measurement devices larger. While this bias shift phenomenon was expected for changes in the laser mode, and confirmed by talking with the ULS manufacturer (LTI, Tom Girmann), the size of the bias shift was much larger than anticipated. This is thought to be attributable to the large scale of disturbing factors which may be present in an open ocean environment such as sea-spray, foam, wave cresting, and wind. The bias difference resulting from the change in laser PRF and PPM settings, while unexpected by both myself and the manufacturer, is also thought to be attributable to the same open ocean factors which result in such a large bias shift due to mode changes. Higher PRF settings may result in a larger number of laser pulses breaking through interfering factors which could cause measurements reading further the laser. Thus a higher PRF would give an increased bias similar to one seen when shifting from averaging to last targeting. Again the magnitude of this bias shift was large, on the same order of magnitude as the shift seen due to the laser mode shift.

Although the bias differences between the laser modes and was not unexpected, based upon the processing characteristics of the laser, the magnitude of the biases was surprising (over 9 cm of bias range between the three modes compared). While presenting an operational challenge, this bias shift phenomena is not prohibitive of the

laser's use for this application. Additional controlled testing should allow the determination of optimal laser settings for the Harvest Platform environment and the determination of an instrumental reference for the laser. Ultimately it was decided to leave the ULS in the first mode (LT mode, PRF 500, PPM 10) to maintain consistency and to extend the life of the laser since higher PRF rates can shorten the laser's expected lifetime.

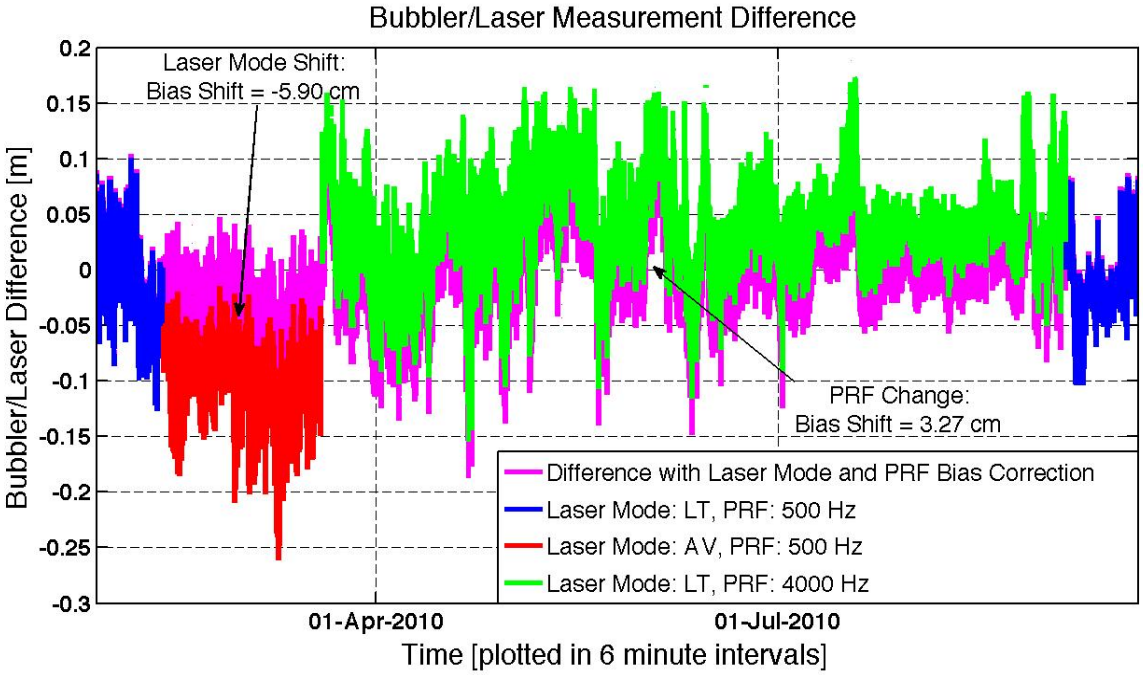

Figure 8: Plot of Bubbler/Laser measurement difference (ΔSSH) showing bias shifts due to changes in laser mode settings (LT = Last Target Mode, AV = Averaging Mode). Note that the underlying purple data depicts the laser data with the appropriate bias correction applied.

7.2. Laser Bench Testing

In order to try and characterize the bias shift resulting from changing the laser mode and settings some bench testing of the laser was performed. It is important to note that the laser used in the testing described is the same make and model as the unit onboard the Harvest platform, however it is not the same unit and thus some differences

may exist between the two. Additionally the results of these bench tests are not fully understood. However, these tests provided some interesting results and are presented here so that the results may be documented and presented as a starting point for future work.

These tests were performed by measuring the laser data output for four different operating settings: Last Target mode at 4000 PRF, Last Target mode at 500 PRF, Averaging mode at 4000 PRF, and Averaging mode at 500 PRF. The PPM settings were changed for each case in order to maintain the same 50 Hz laser output that is used onboard the Harvest platform. These tests were then conducted at two distances of approximately 2.44 m (short) and 12.2 m (long). The 12.2 meter distance was selected because this is approximately the average distance measured at the platform. 4000 measurements were taken for each setting at each distance, the results of which are presented below in Tables 2, 3, 4, and 5.

	Mean [m]	**Taped – Mean [m]**	**Standard Deviation [m]**	**Max [m]**	**Min [m]**	**Max – Min [m]**
Last Targeting 4000 PRF	12.1870	-0.0153	0.0116	12.2980	12.1800	0.1180
Last Targeting 500 PRF	12.1861	-0.0162	0.0094	12.2170	12.1790	0.0380
Averaging 4000 PRF	12.1749	-0.0274	0.0092	12.2220	12.1370	0.0850
Averaging 500 PRF	12.1829	-0.0194	0.0040	12.1950	12.1570	0.0380

Table 2: Results for long distance laser bench test. Note the actual taped distance is 12.2023 m

	Mean [m]	Taped – Mean [m]	Standard Deviation [m]	Max [m]	Min [m]	Max – Min [m]
Last Targeting 4000 PRF	2.4632	0.0208	0.0083	2.5800	2.4310	0.1490
Last Targeting 500 PRF	2.4583	0.0159	0.0053	2.4640	2.4250	0.0390
Averaging 4000 PRF	2.4301	-0.0123	0.0056	2.4770	2.4030	0.0740
Averaging 500 PRF	2.4360	-0.0064	0.0074	2.4620	2.4170	0.0450

Table 3: Results for short distance laser bench test. Note the actual taped distance is 2.4424 m

Difference of means [m]	Last Targeting 500 PRF	Averaging 4000 PRF	Averaging 500 PRF
Last Targeting 4000 PRF	0.0009	0.0121	0.0041
Last Targeting 500 PRF		0.0112	0.0032
Averaging 4000 PRF			-0.0080

Table 4: Bias differences between laser setting for long distance laser bench test. Note the actual taped distance is 12.2023 m.

Difference of means [m]	Last Targeting 500 PRF	Averaging 4000 PRF	Averaging 500 PRF
Last Targeting 4000 PRF	0.0049	0.0331	0.0272
Last Targeting 500 PRF		0.0282	0.0223
Averaging 4000 PRF			-0.0059

Table 5: Bias differences between laser setting for short distance laser bench test. Note the actual taped distance is 2.4424 m.

We can immediately see that the biases between the different modes at the longer distance (which is approximately the distance measured at the Harvest platform) are approximately one order of magnitude smaller than the bias shifts detected at the platform (see Figure 8). The reasoning for this large discrepancy is unknown but environmental factors such as sea-spray, foam, wave cresting, and wind are thought to play a significant role.

Some additional observations may be made from the data above. Generally the biases between modes are larger for the shorter measurement distance (with the exception of comparing Averaging in 500 and 4000 PRF). This seems counter-intuitive and one would generally think that the bias would increase as measured distance increases. Also, in general the data are noisier, as indicated by the standard deviation of the data, with increased measurement distance (except for the Averaging 500 PRF setting where the standard deviation of the data went down). This is shown below in Figure 9 and 10. Of curious note, the Last Targeting 500 PRF setting exhibits a different behavior for the two distances, which can be seen visually in Figures 9 and 10 below. For this mode, the laser noise seems to bias the measurement closer for the shorter distance and further out for the longer distance. Again, the results of these bench tests are not fully understood but are shown here so that the results may be documented and presented as a starting point for future work which should include laser testing at a greater variety of PRF settings as well as distances to try and further understand the phenomena seen in these bench tests.

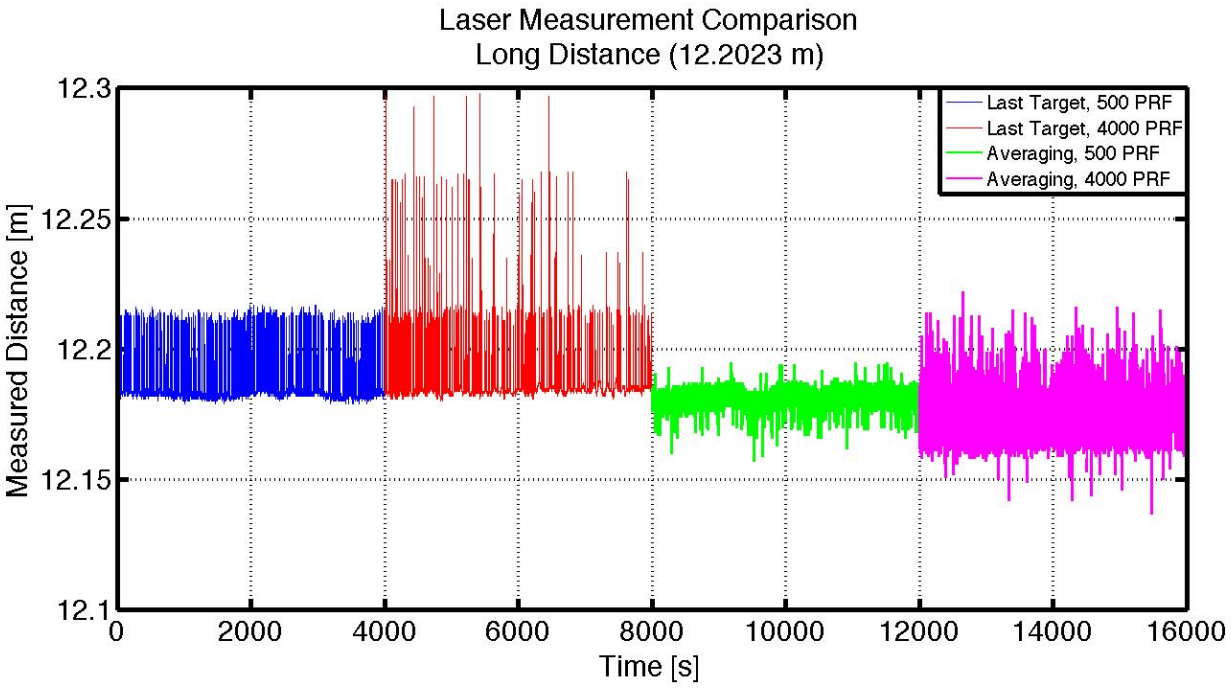

Figure 9: Plot of 50 Hz laser measurements for long distance bench testing. Note the actual taped distance is 12.2023 m.

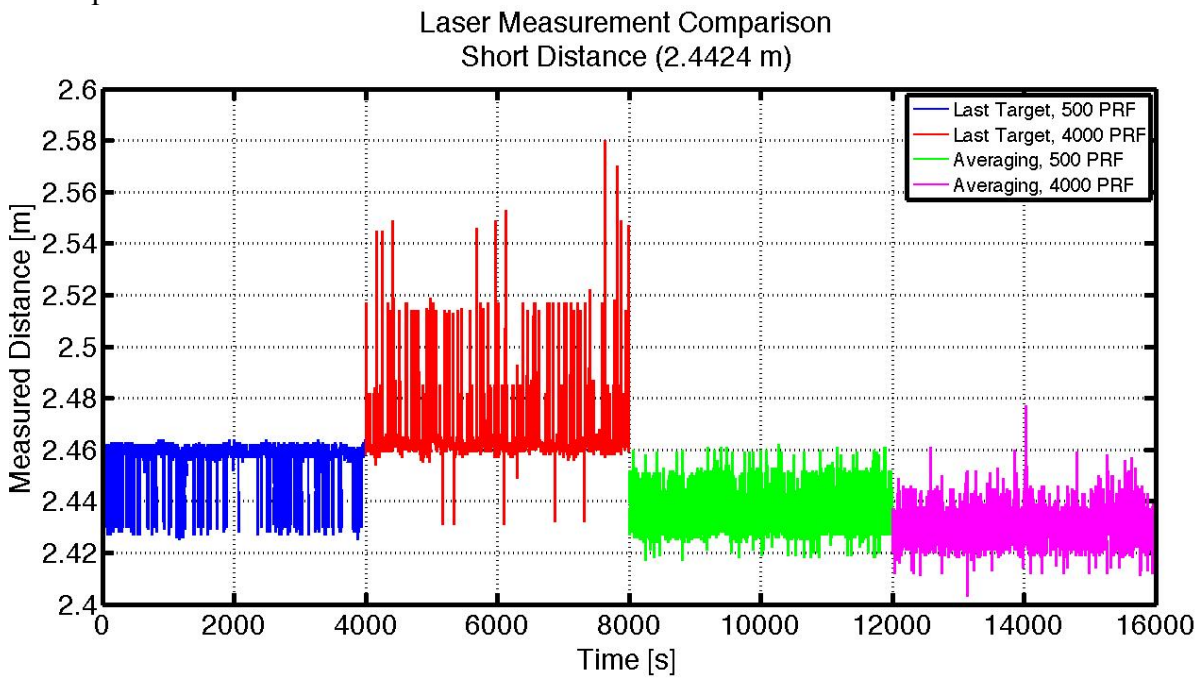

Figure 10: Plot of 50 Hz laser measurements for short distance bench testing. Note the actual taped distance is 2.4424 m.

8. Regression and Filtering

8.1. Initial Filtering

Initially plotting the difference between the bubbler and laser measurements shows that there are significant outliers present in the data (as can be seen in Figure 11 below). The laser data includes some filtering in the software processing of the raw data to remove obviously erroneous data. This includes 1 Hz measurements which have a range greater than 3 m; a mean less than 8m, meaning that the laser is reading significantly shorter than reasonably expected; or a mean greater than 20m, meaning the reading is significantly longer than expected.

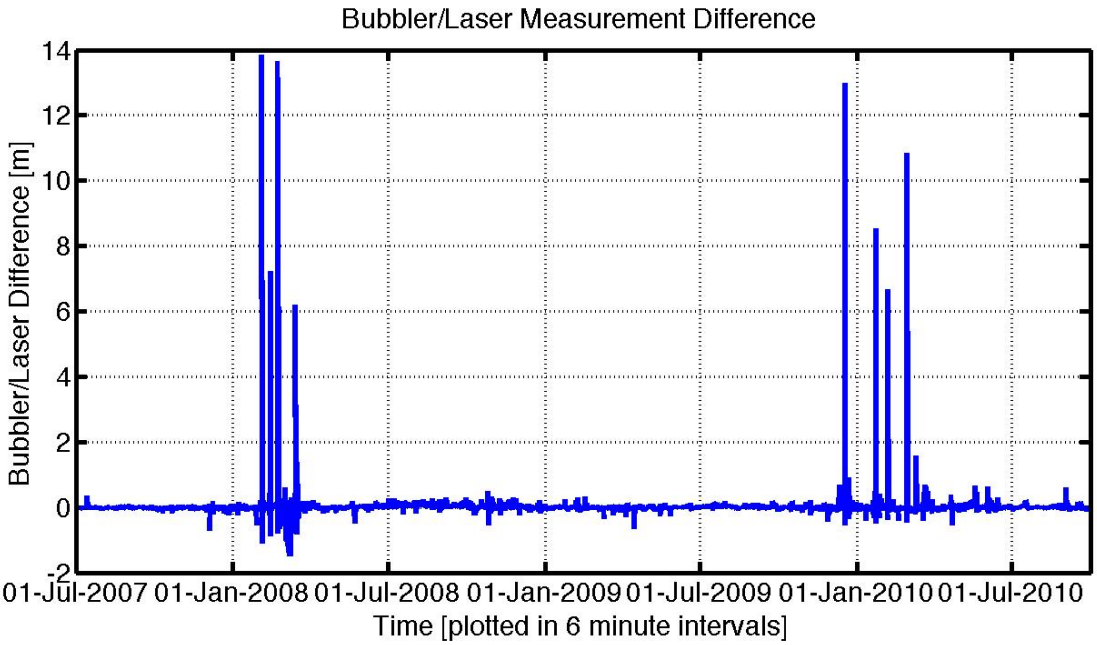

Figure 11: Bubbler/Laser Measurement Difference with no filtering applied.

It was noted that there is a strong relationship between the measurement difference and the 1 Hz percent return average, as shown in Tables 6 and 7 and Figure 12

below. Thus an additional filter was added to the laser to remove laser 6-minute data points which fall below a defined 1 Hz return average threshold of 95%. This threshold was selected because it resulted in a low remaining rms error (4.22 cm) while retaining a largest percentage of data. This resulted in removal of approximately 13.7% of the given data, with 86.3% of the total time series remaining. Thresholds above 95% could have been selected but this resulted in a significant amount of data being removed (greater than 12%) with minimal reduction in the rms error.

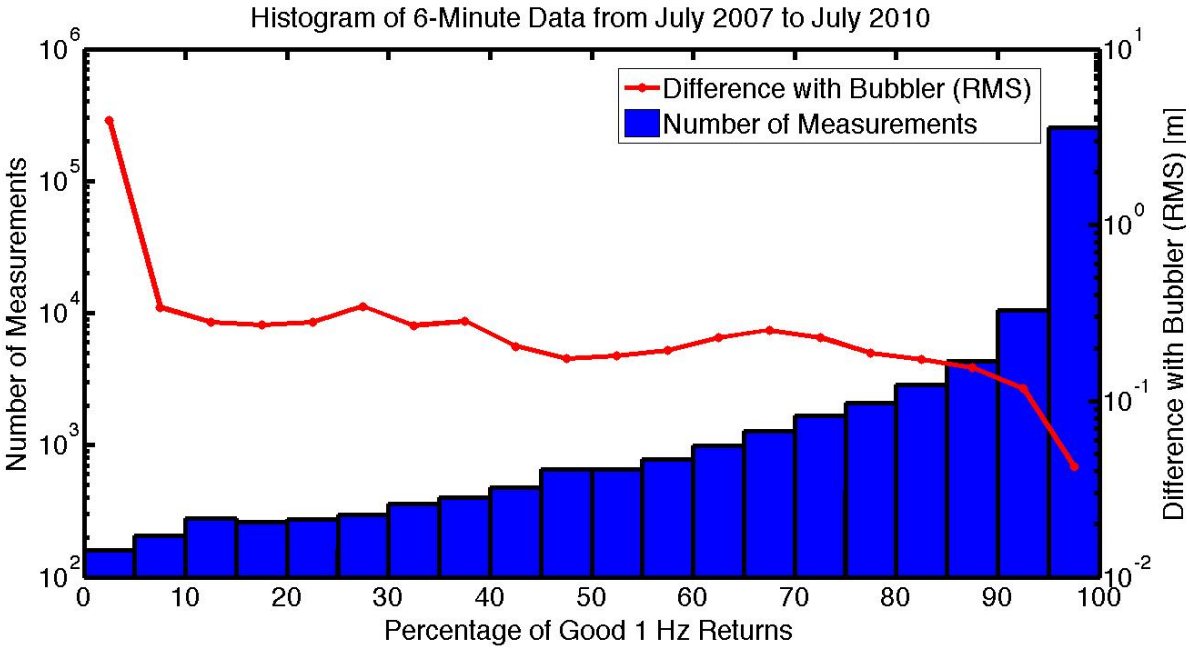

Figure 12: Histogram of 6-minute data showing the percentage of good 1 Hz returns with the rms error for each histogram bin shown in red.

Percentage of Good 1 Hz Returns [%]	RMS error of associated Good 1 Hz Return bin [cm]	Percentage of total time-series of 6-minute data [%]
0 - 5	394.8	0.1
5 - 10	34.1	0.1
10 - 15	27.9	0.1
15 - 20	27.1	0.1
20 - 25	28.1	0.1
25 - 30	34.6	0.1
30 - 35	26.8	0.1
35 - 40	28.4	0.1
40 - 45	20.4	0.2
45 - 50	17.4	0.2
50 - 55	18.0	0.2
55 - 60	19.3	0.3
60 - 65	22.9	0.3
65 - 70	25.3	0.4
70 - 75	23.0	0.6
75 - 80	18.7	0.7
80 - 85	17.2	1.0
85 - 90	15.4	1.5
90 - 95	11.8	3.7
95 - 100	4.2	88.5

Table 6: Filtering properties of percentage Good 1 Hz Return parameter

Percentage of Good 1 Hz Returns [%]	RMS error of associated Good 1 Hz Return bin [cm]	Percentage of total time-series of 6-minute data [%]
95 - 100	4.2	88.5
96 - 100	4.1	86.6
97 - 100	4.0	83.2
98 - 100	3.8	76.2
99 - 100	3.5	52.5

Table 7: Filtering properties of percentage Good 1 Hz Return parameter for intervals above 95%.

Despite the effectiveness of removing outliers based upon the 1 Hz return rate as an indication of laser performance, some outliers still exist within the time-series analyzed, but at a considerably reduced magnitude. In order to remove these a 3σ filter was applied, which removed any data points outside of these bounds based upon a moving-mean "boxcar" average. Ultimately a 3σ filter using a 10-day moving average was utilized. The 10-day moving interval was selected in order to remove large, obvious outliers while retaining as much data as possible. Selecting a shorter interval for the boxcar resulted large outlier segments being retained while discarding less obvious deviations which could possibly provide useful data correlation. The selected filter removed an additional 0.7% of the full time-series leaving 87.8% of the full time-series remaining. This also reduced the rms error from 4.22 cm to 3.78 cm.

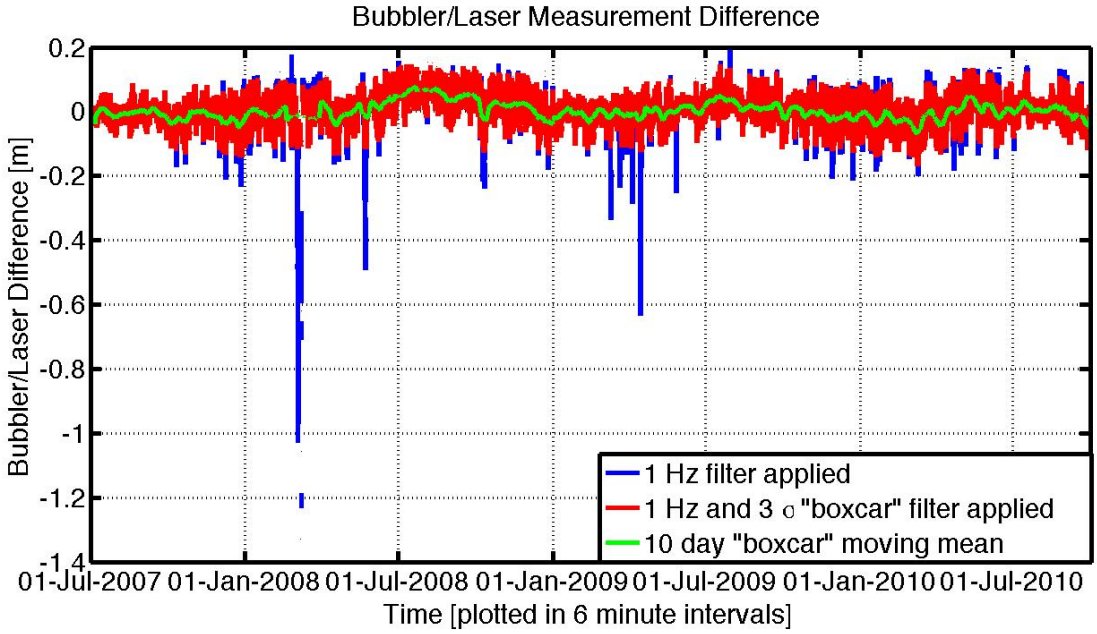

Figure 13: Results of 3σ, 10 day moving mean "boxcar" filter on the Bubbler/Laser difference.

8.2. Post Filtering

After the initial filtering to remove outliers, the data still demonstrate very noisy behavior which appears to have some systematic trends within it. Subsequent analysis then focused on identifying the causes of deviations in the laser bubbler measurements and compensating for these.

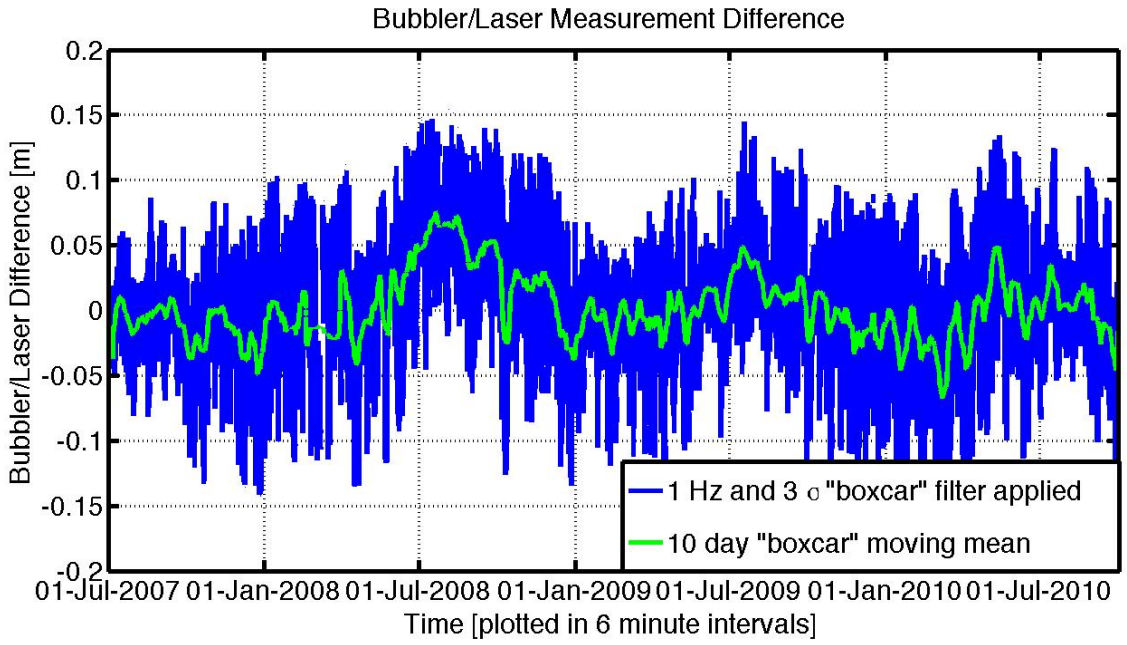

Figure 14: Results of 3σ, 10 day moving mean "boxcar" filter on the Bubbler/Laser difference (close up of Figure 13).

One initial thought about what may be contributing to the measurement variation between the devices is variation in the vertical separation of the instruments. This could be due to mechanical movement of the platform as a result of a variety of influences. Unfortunately, no accurate survey of the laser location has been conducted, so the vertical separation of the units must be estimated, but it is known to be approximately 27 m. Some variation in this vertical separation can be attributed to loading and thermal effects, however these are estimated to be 0.2 – 2.0 mm (Haines et al., 2003) for the entire

structure, which is over 240 m tall, and thus are considered negligible for the 27 m of separation between the instruments. Additionally, the units are not located directly over one another, but their horizontal separation is considered negligible since water-level measurements are being compared over an average of 3 minutes worth of 1 Hz data.

8.3. Spectral Analysis

In order to determine what might be affecting or the cause of the systematic differences between the measurement devices, a spectral analysis was conducted on the time-series of the measurement difference between the bubbler and the laser to determine what periodic signals may be present in the data. Due to missing segments of data in the time-series (due to filtering or otherwise) a classical Fourier analysis using the Fast-Fourier Transform (FFT) cannot be performed. Therefore the Lomb-Scargle method was utilized. The Lomb-Scargle method is a spectral analysis method, developed by Lomb (1976) and elaborated on by Scargle (1982), which allows missing segments of data in a time series frequency analysis. A brief summary of the Lamb-Scargle method follows.

In spectral analysis the basic problem considered is there is a physical parameter X that is being measured at times t_i, forming the time series $\{X(t_i),\ i = 1, 2, \ldots N_o\}$. This parameter X is assumed to be the sum of a period signal and random measurement errors.

$$X_i = X(t_i) = X_s(t_i) + R(t_i) \qquad \textbf{Eq. 2}$$

The Lomb-Scargle Periodogram is then defined as the function:

$$P_X(\omega) = \frac{1}{2}\left\{ \frac{\left[\sum_j X_j \cos\omega(t_j - \tau)\right]^2}{\sum_j X_j \cos\omega(t_j - \tau)} + \frac{\left[\sum_j X_j \sin\omega(t_j - \tau)\right]^2}{\sum_j X_j \sin\omega(t_j - \tau)} \right\} \qquad \textbf{Eq. 3}$$

where τ is defined by:

$$\tan(2\omega\tau) = \left(\sum_j \sin 2\omega t_i\right) \Big/ \left(\sum_j \cos 2\omega t_i\right) \qquad \textbf{Eq. 4}$$

This function can be evaluated for any value of the frequency ω. If *X* contains a sinusoidal component of the frequency ω_o, then at and near $\omega = \omega_o$ the sin and cos terms of the equation are in phase and make large contributions to P_X. At other values of ω, the sums are randomly positive and negative and the resulting sums cancel yielding a low value of P_X. This can be viewed as a least-squares fit of a sinusoidal function.

Although the periodogram function can be evaluated at any frequency, it is prudent to limit the spectrum analyzed. This is done by looking at specific range of frequencies. The lower bound is what is known as the fundamental frequency $\omega_1 = 2\pi/T$, which corresponds to a sine wave of a period equal to the span of the whole time series interval, T. For this analysis the period T is equal to 3 years. The upper frequency bound is defined by the Nyquist frequency $\omega_N = \pi/\Delta t$, where Δt is the sampling interval which is approximately the highest frequency about which information is available because it is the shortest interval spanned. For this analysis the sampling interval is 6 minutes.

The Lomb-Scargle spectral analysis method was implemented using a Matlab code based upon the code found in Numerical Recipes in C: the Art of Scientific Computing (2007). This resulted in several short and long period frequencies being found in the data shown below in Figures 15, 16, and 17. The short period signals (on the order of hours) in Figure 15 demonstrate a strong 24 hour signal. This suggests dependence of one of the instruments on a diurnal influence such as tide, temperature, or barometric pressure. Moving to slightly longer period signals, on the order of days, we can see in Figure 16 that there is a strong signal present with a periodicity of approximately 27 days indicating a strong tidal or water sea-surface height effect on the instrument difference. Finally, Figure 17 shows the spectral density for signals with periods on the order of years. We can see that there is a strong spectral component with a signal period just slightly longer than one year. This suggests annual seasonal effects such as sea-state (a combination of wave height and wind conditions) and temperature.

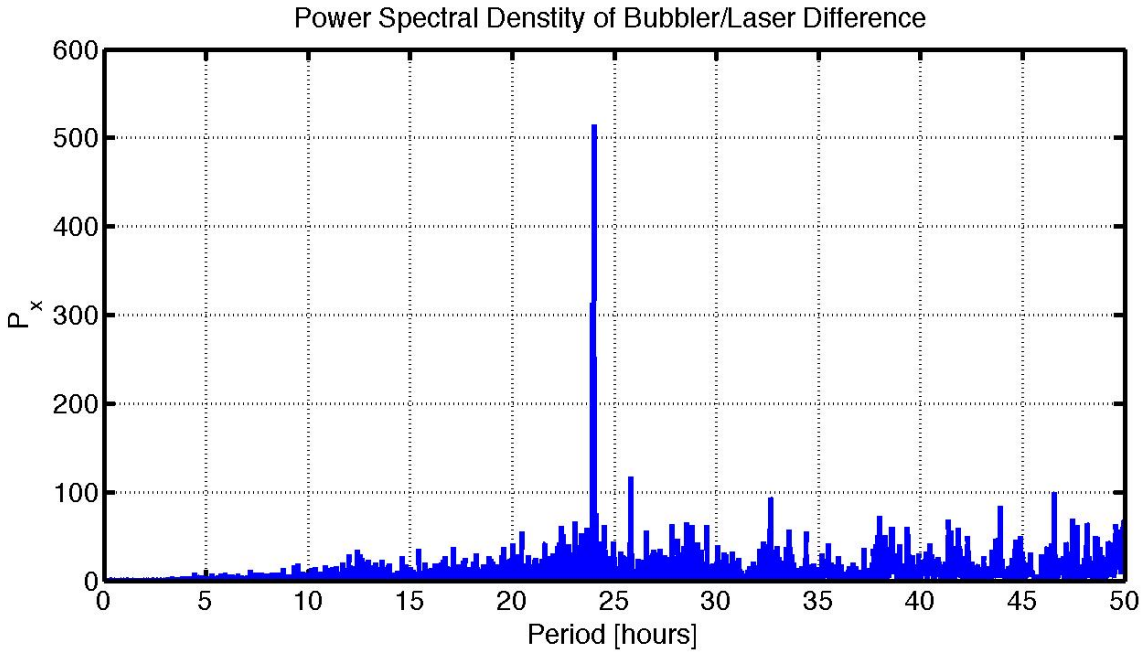

Figure 15: Short Period (hours) Lomb-Scargle Periodogram results for Period range of 0 – 50 hours.

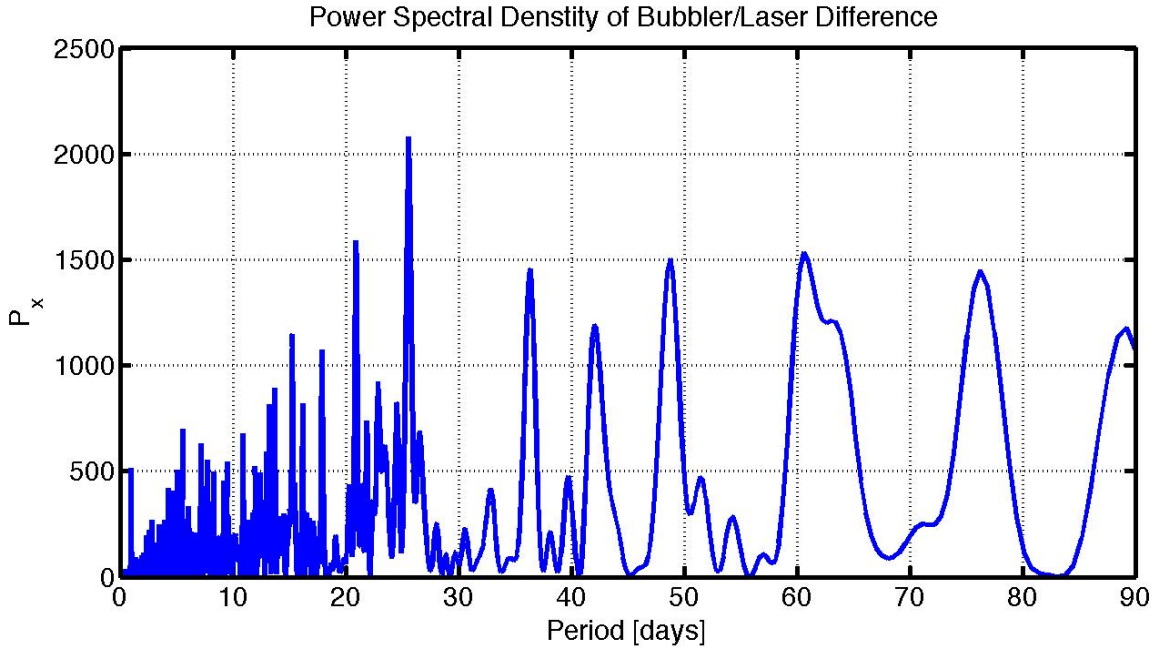

Figure 16: Medium Period (days) Lomb-Scargle Periodogram results for Period range of 0 – 90 days.

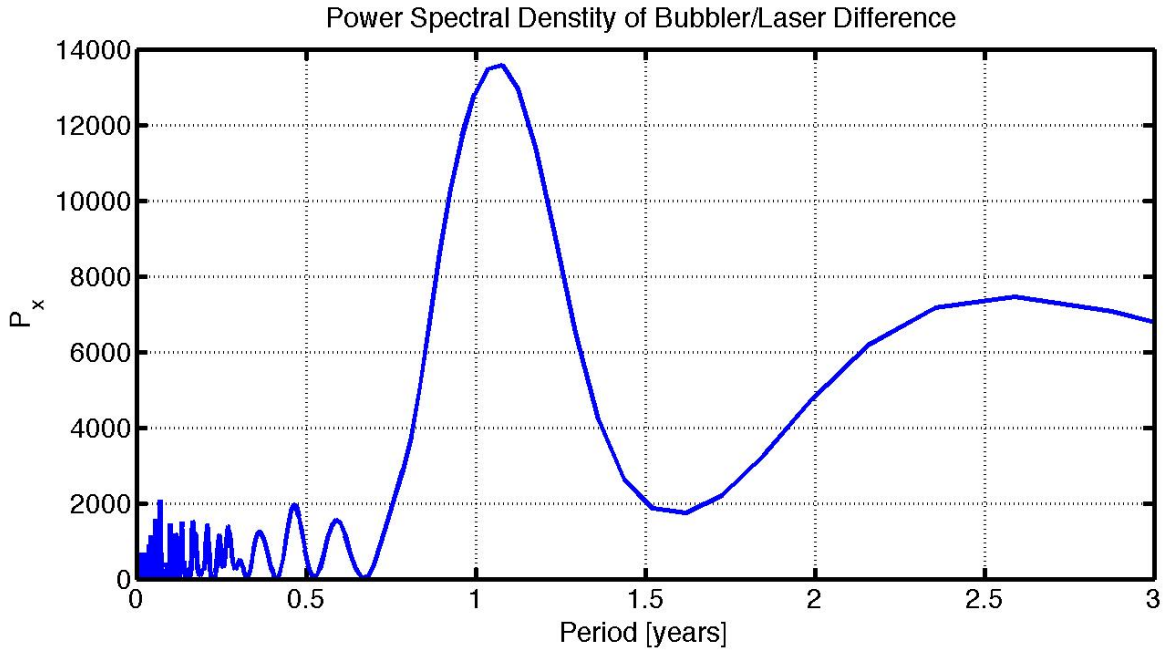

Figure 17: Long Period (years) Lomb-Scargle Periodogram results for Period range of 0 – 3 years.

Although this frequency analysis provided some insight into the possible influences on the instrument differences, it did not specifically indicate any one influence. Additionally, due to the fact that the time-series is only three years long, signals with periods greater than 1.5 years have suspect determination utilizing frequency analysis.

8.4. Influencing Effects

From looking at the Bubbler/Laser measurement difference plot it appears as though there is some periodic influence driving the difference between these two instruments. The spectral analysis discussed in the previous section confirms this and implies that these may be due to diurnal, tidal/water height, and long term seasonal factors. We then began to look into different environmental parameters that may influence the difference. Just by plotting these factors over the period being investigated several of these parameters display trends which appear to correlate with those seen in the Bubbler/Laser measurement difference. The environmental parameters for which data is available are shown below in Figures 18 through 23.

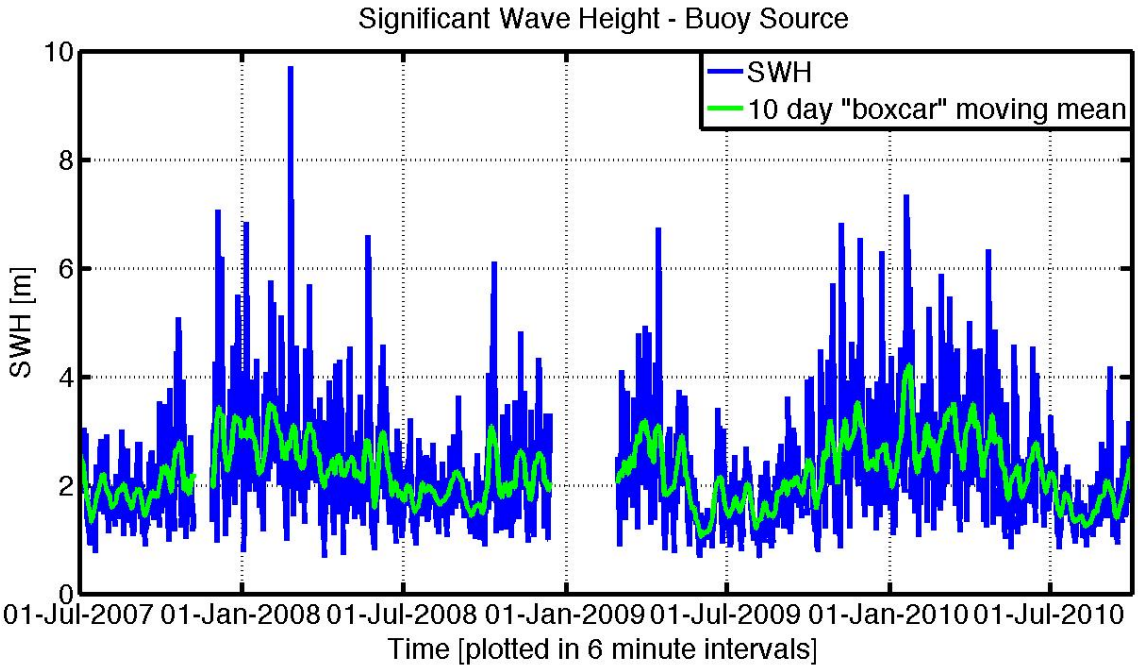

Figure 18: SWH data from NOAA CDIP buoy source over the time series.

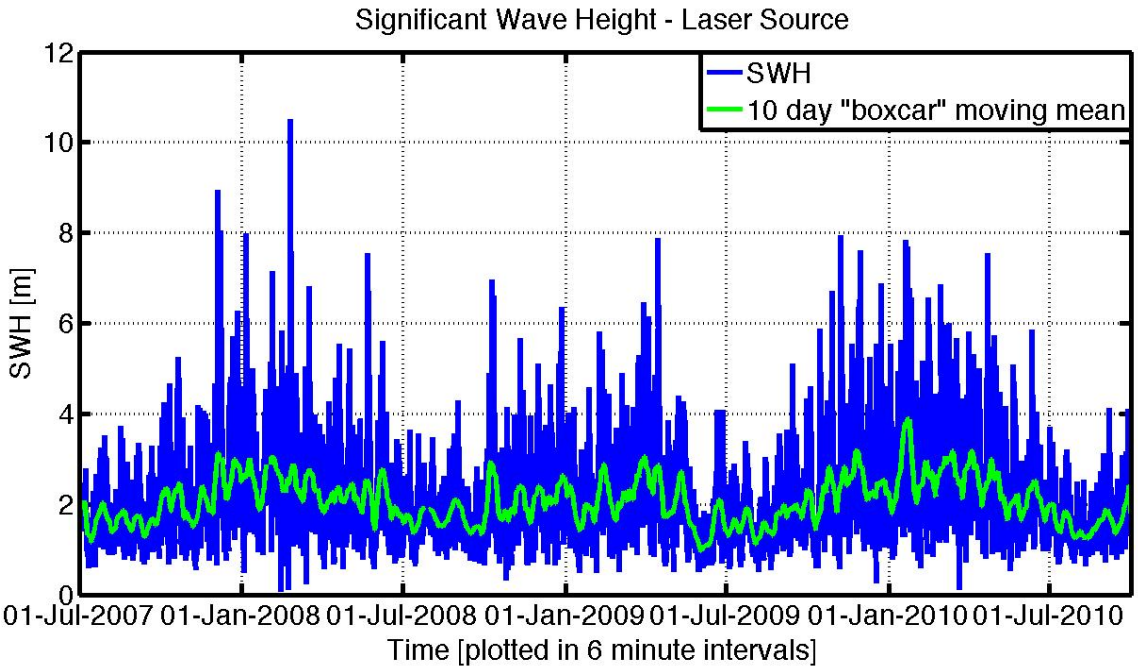

Figure 19: SWH data from the Harvest laser over the time series.

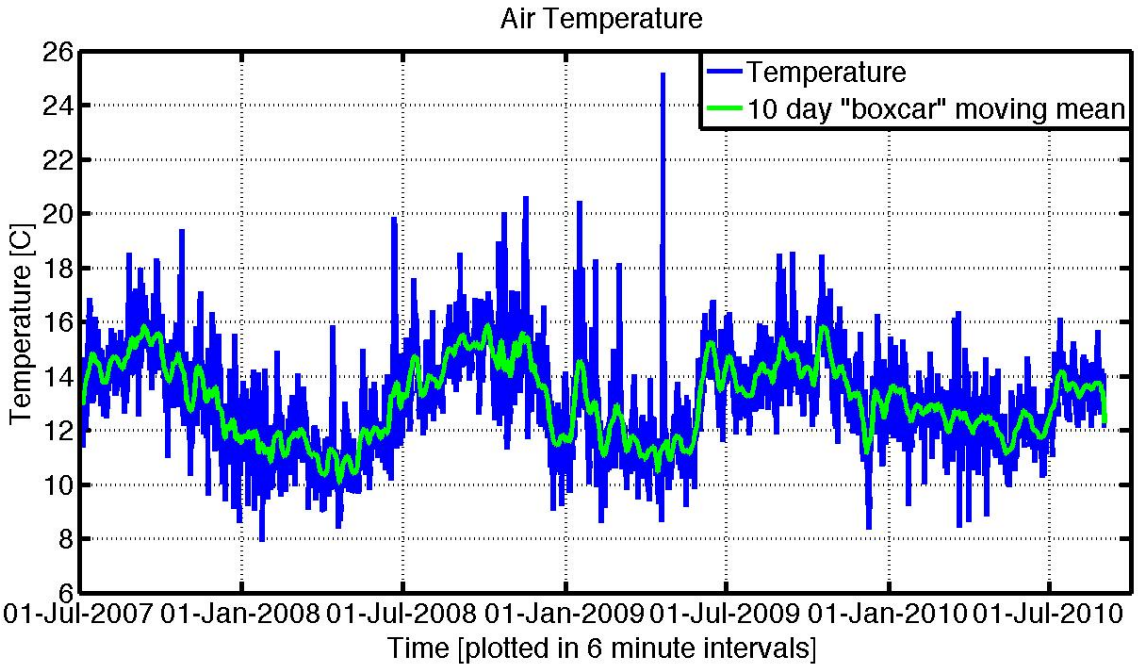

Figure 20: Air temperature data from NOAA NDBC buoy source over the time series.

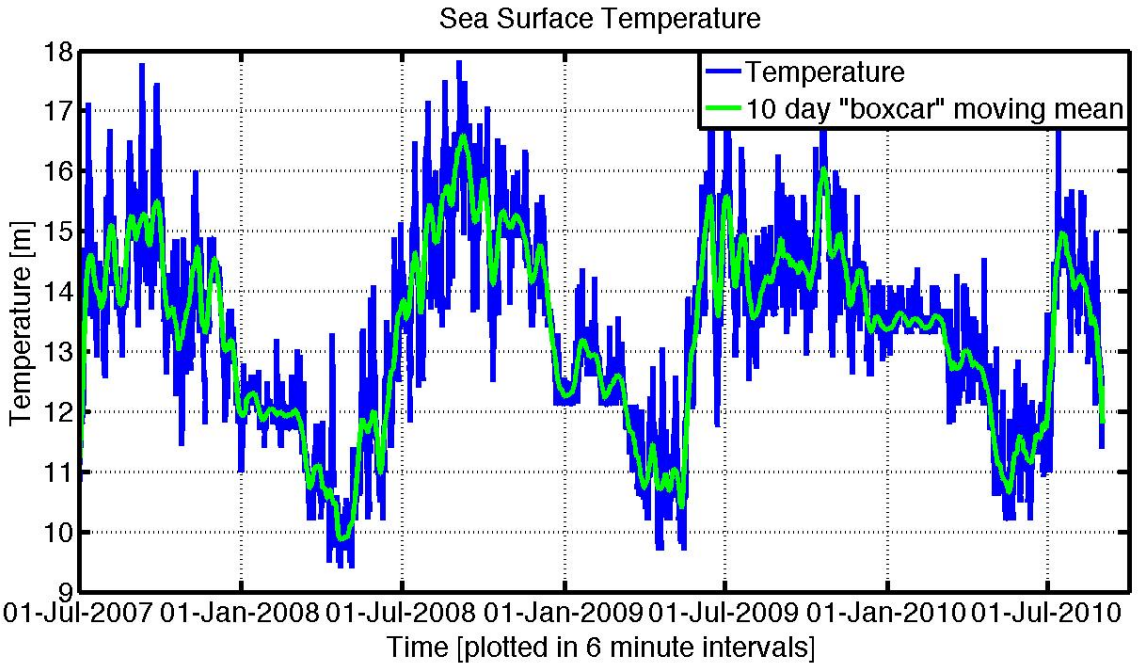

Figure 21: Sea Surface temperature data from NOAA NDBC buoy source over the time series.

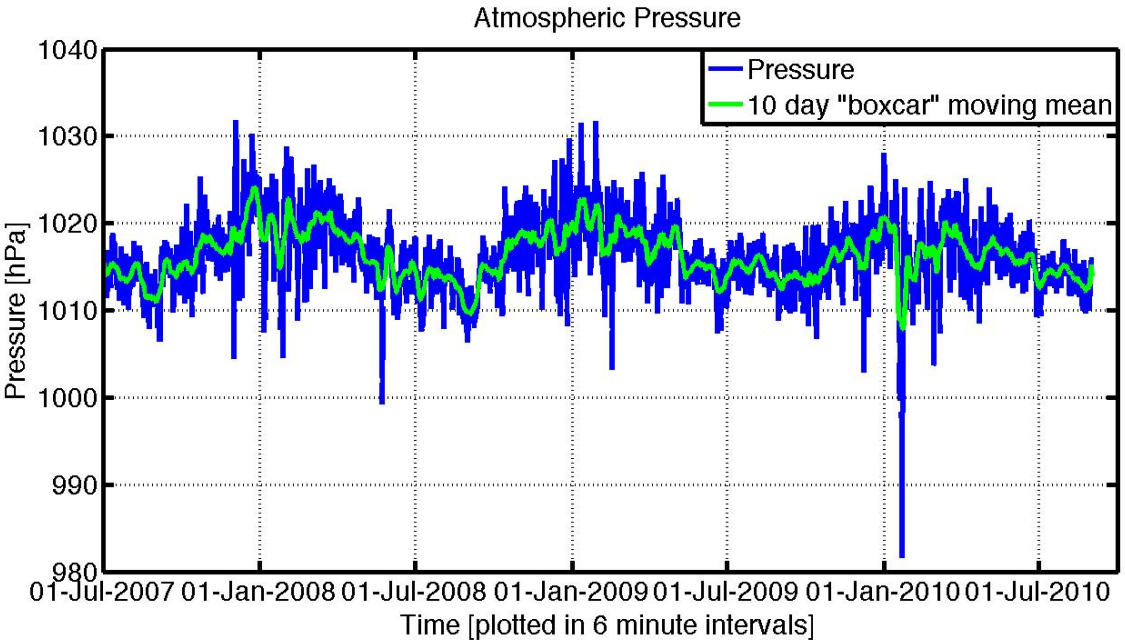

Figure 22: Atmospheric pressure data from NOAA NDBC buoy source over the time series.

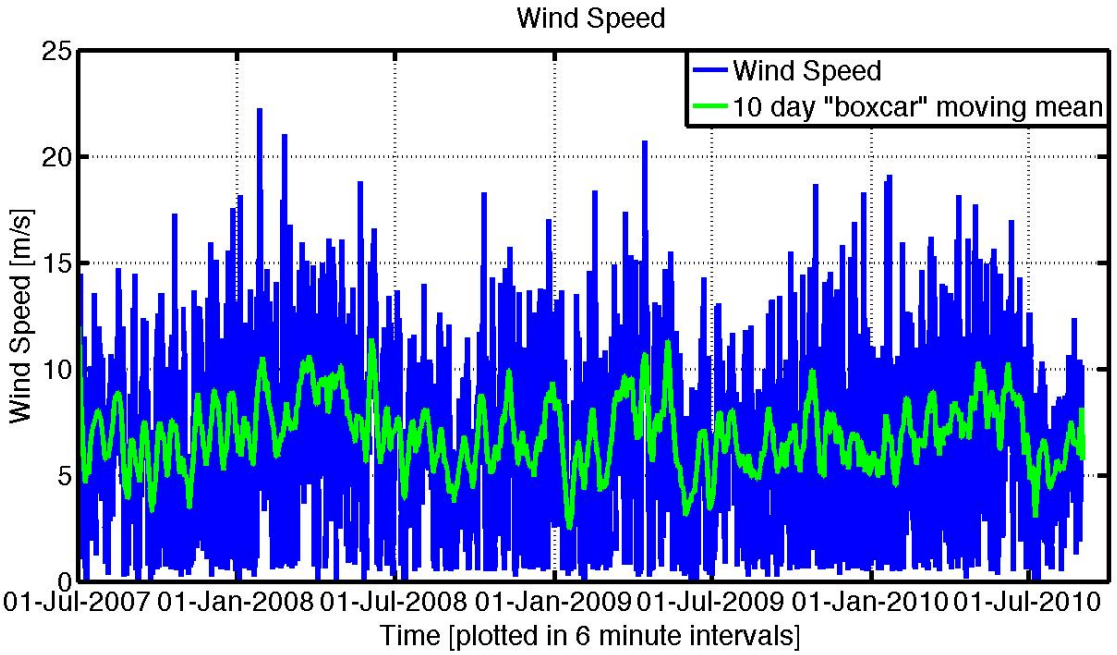

Figure 23: Wind speed data from NOAA NDBC buoy source over the time series.

8.5. Regression

8.5.1. Discussion of Least Squares

For the purposes of this paper we will provide a brief overview of the linear least-squares method and how it is applied to the subsequent regression analyses performed for this paper. The least squares method seeks to find an estimate of a given set of values which minimize the sum of the square of the residuals for an over-determined system (i.e. more equations/measurements than unknowns). For this analysis we will be estimating values for a linear correction coefficient which, when multiplied by the associated parameter, minimizes the Bubbler/Laser measurement difference (residual). Thus we begin with the following equations.

$$\Delta SSH = SSH_{Bubbler} + SSH_{Laser} - SSH_{Correction} \quad \textbf{Eq. 5}$$

$$SSH_{Correction} = B_0 + B_1 \times Paramter_1 + B_2 \times Paramter_2 + \ldots B_n \times Paramter_n \quad \textbf{Eq. 6}$$

It is important to note that the laser is downward facing, thus its measurements are positive. In order to determine the difference between the bubbler and laser, we can add these values together and then subtract the vertical separation between the instruments. Since this value is not known exactly we will estimate it during the least squares regression using the constant B_0. Coefficients $B_1 – B_n$ are the n linear correction coefficients which we will be estimating. To utilize common least squares notation we will make the following definitions:

$$Y(t) = SSH_{Bubbler}(t) + SSH_{Laser}(t) \quad \textbf{Eq. 7}$$

$$\varepsilon(t) = \Delta SSH(t) \qquad \textbf{Eq. 8}$$

Where Y(t) is the uncorrected Measurement Difference and ε(t) is the measurement residual at time t for times 1 - m. We will write the time series of Y(t) and ε(t) in matrix form **Y** and **ε** respectively.

$$\mathbf{Y} = \begin{bmatrix} \mathrm{Y}(1) \\ \mathrm{Y}(2) \\ \vdots \\ \mathrm{Y}(\mathrm{m}) \end{bmatrix}, \quad \boldsymbol{\varepsilon} = \begin{bmatrix} \varepsilon(1) \\ \varepsilon(2) \\ \vdots \\ \varepsilon(\mathrm{m}) \end{bmatrix} \qquad \textbf{Eq. 9 and 10}$$

We may then define the $SSH_{Correction}$ term as the product of two matrices, one which is an m x n matrix containing n columns of the time series data of each parameter being evaluated, the other is a n x 1 matrix containing the linear correction coefficients being estimated.

$$SSH_{Correction} = \mathbf{HX} \qquad \textbf{Eq. 11}$$

$$\mathbf{H} = \begin{bmatrix} 1 & \mathrm{Parameter}_1(1) & \mathrm{Parameter}_2(1) & \cdots & \mathrm{Parameter}_n(1) \\ 1 & \mathrm{Parameter}_1(2) & \mathrm{Parameter}_2(2) & \cdots & \mathrm{Parameter}_n(2) \\ \vdots & \vdots & \vdots & \ddots & \vdots \\ 1 & \mathrm{Parameter}_1(\mathrm{m}) & \mathrm{Parameter}_2(\mathrm{m}) & \cdots & \mathrm{Parameter}_n(\mathrm{m}) \end{bmatrix} \qquad \textbf{Eq. 12}$$

$$\mathbf{X} = \begin{bmatrix} \mathrm{B}_0 \\ \mathrm{B}_1 \\ \vdots \\ \mathrm{B}_n \end{bmatrix} \qquad \textbf{Eq. 13}$$

Thus we may define the following matrix equation.

$$\boldsymbol{\varepsilon} = \mathbf{Y} - \mathbf{HX} \qquad \textbf{Eq. 14}$$

The least squares method solution minimizes the residuals in $\boldsymbol{\varepsilon}$ by selecting the values of **X** which minimize the performance index J defined below.

$$\mathbf{J(X)} = \frac{1}{2}\boldsymbol{\varepsilon}^{\mathbf{T}}\boldsymbol{\varepsilon} = \frac{1}{2}\mathbf{(Y - HX)}^{\mathbf{T}}\mathbf{(Y - HX)} \qquad \textbf{Eq. 15}$$

By taking the first derivative of the performance index J and setting it equal to zero, we may then find the minimum of J.

$$\frac{\partial \mathbf{J}}{\partial \mathbf{X}} = 0 = -\mathbf{H}^{\mathbf{T}}\mathbf{(Y - HX)} \qquad \textbf{Eq. 16}$$

Therefore we can solve for the best estimate of **X**, which we will denote $\hat{\mathbf{X}}$.

$$\mathbf{(H^T H)\hat{X} = H^T Y} \qquad \textbf{Eq. 17}$$

$$\mathbf{\hat{X} = (H^T H)^{-1} H^T Y} \qquad \textbf{Eq. 18}$$

Thus we can determine a correction which may be applied to the Bubbler/Laser measurement difference. There are more rigorous mathematical restrictions placed upon the least-squares derivation than what is described here, however these are beyond the intent and scope of this paper and we will suffice to say that these conditions are met. We also define the additional matrix, known as the variance-covariance matrix **P**.

$$\mathbf{P = (H^T H)^{-1}} \qquad \textbf{Eq. 19}$$

This matrix contains a great deal of information on the least squares estimation performed, particularly the estimation error associated with **X**. The diagonals of **P** contain the variances (σ_i^2) of **X** and the off diagonal terms contain the covariances (μ_{ij}) of **X**. The covariance contains information on the degree of linear correlation between estimated parameters in **X**, called the correlation coefficient, which is defined below.

$$\rho_{ij} = \frac{\mu_{ij}}{\sigma_i \sigma_j} \qquad \textbf{Eq. 20}$$

Thus we may show that P is:

$$\mathbf{P} = \begin{bmatrix} \sigma_1^2 & \mu_{12} & \cdots & \mu_{1n} \\ \mu_{12} & \sigma_2^2 & \cdots & \mu_{2n} \\ \vdots & \vdots & \ddots & \vdots \\ \mu_{1n} & \mu_{2n} & \cdots & \sigma_n^2 \end{bmatrix} = \begin{bmatrix} \sigma_1^2 & \rho_{12}\sigma_1\sigma_2 & \cdots & \rho_{1n}\sigma_1\sigma_n \\ \rho_{12}\sigma_1\sigma_2 & \sigma_2^2 & \cdots & \rho_{2n}\sigma_2\sigma_n \\ \vdots & \vdots & \ddots & \vdots \\ \rho_{1n}\sigma_1\sigma_n & \rho_{2n}\sigma_2\sigma_n & \cdots & \sigma_n^2 \end{bmatrix} \qquad \textbf{Eq. 21}$$

For ease of presentation, the **P** matrix will subsequently be presented in the following form which shows the square-root of the variance along the diagonals and only the correlation coefficient in the upper diagonal terms.

$$\mathbf{P} = \begin{bmatrix} \sigma_1 & \rho_{12} & \cdots & \rho_{1n} \\ & \sigma_2 & \cdots & \rho_{2n} \\ & & \ddots & \vdots \\ & & & \sigma_n \end{bmatrix} \qquad \textbf{Eq. 22}$$

8.5.2. Individual Parameter Regression

Since many of the above parameters displayed similar periodic trends to those found in the Bubbler/Laser measurement difference we next tried a simple linear least-squares regression of the Bubbler/Laser measurement difference against each individual parameter to determine a possible correlation. The linear least squares regression was used to determine a linear correction factor for each parameter utilizing the following equation.

$$Y(t) = B_0 + B_1 * Parameter(t) \qquad \textbf{Eq. 23}$$

In addition to the environmental parameters described previously we also investigated regressing against the average 50 Hz return percentage as described in Section 4.2. This parameter serves as a proxy for laser performance and thus could prove a useful regression parameter for correction to the laser. A Histogram of the average 50 Hz return average is shown in Figure 24 as well as a plot of the parameter over the time series analyzed in Figure 25. The results of the regression analysis performed using each parameter individually are shown below in Table 8.

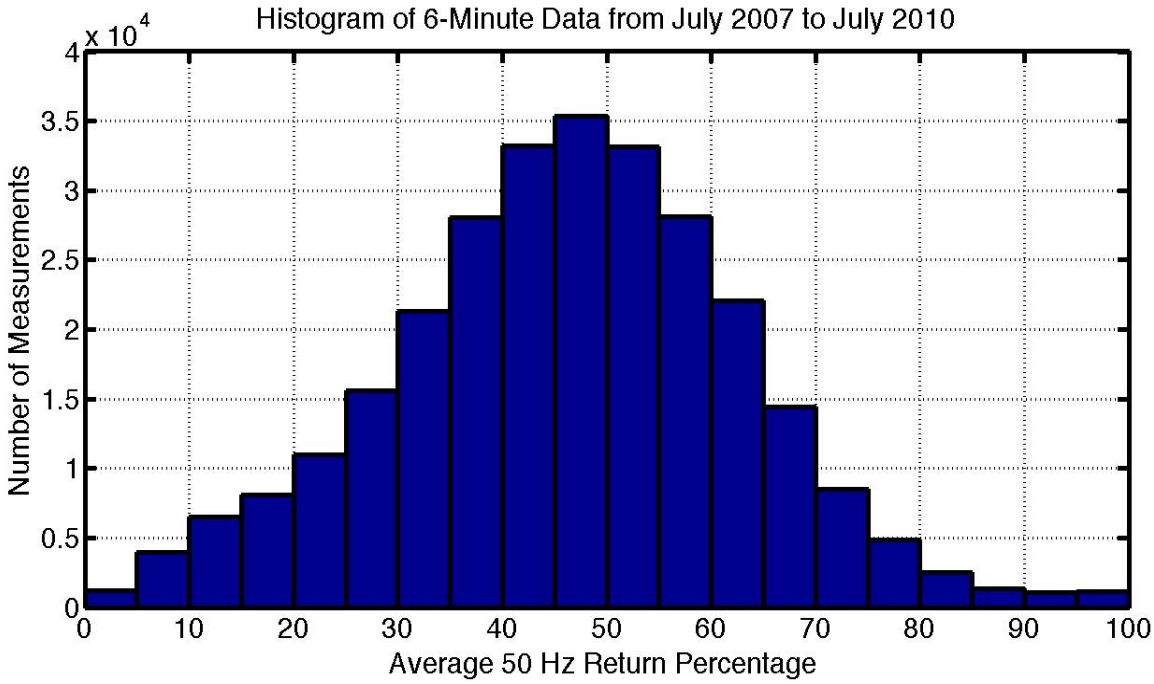

Figure 24: Histogram of 6-minute data showing the average 50 Hz return percentage.

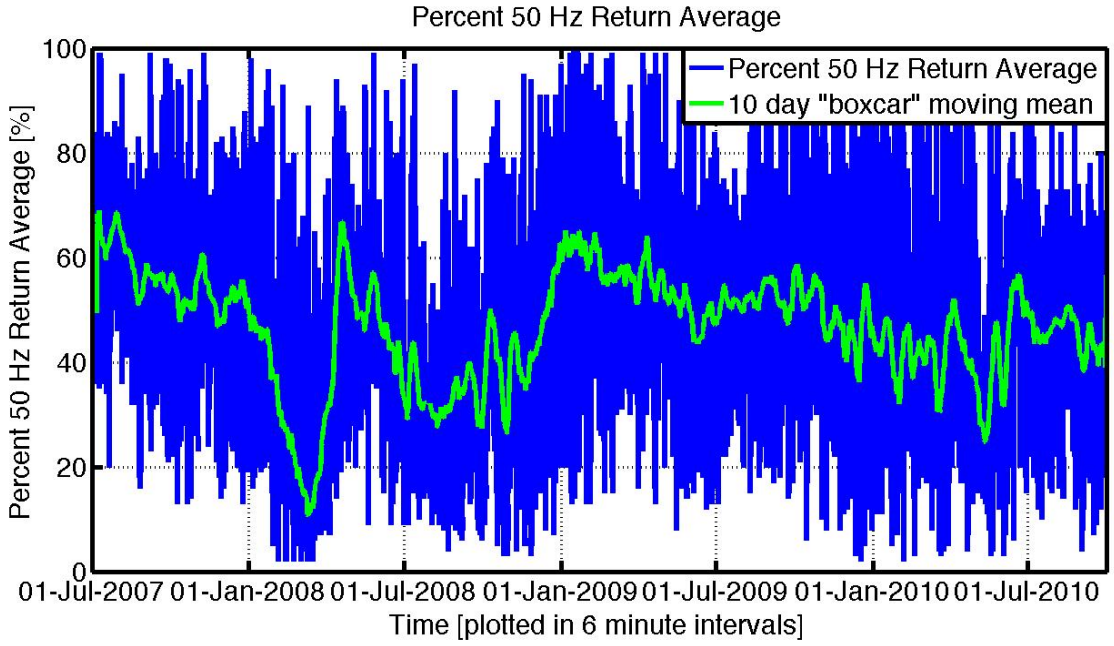

Figure 25: Average 50 Hz return percentage data from the laser over the time series.

Parameter	Coefficient	Sqrt of coefficient variance [cm]	RMS [cm]	Δ RMS (reduction) [cm]	Percent of original time series data
Original			3.78		87.8
SWH (buoy)	-0.0234	0.0023	3.22	0.56	80.1
SWH (laser)	-0.0245	0.0024	3.16	0.62	87.8
Air Temp	0.0049	0.0012	3.69	0.09	84.9
Sea Surface Temp	0.0052	0.0013	3.70	0.08	83.9
Atm Pressure	-0.0007	0.0005	3.78	0.00	84.1
Wind Speed	-0.0017	0.0006	3.73	0.05	85.5
50 Hz Parameter	-0.0010	0.0001	3.53	0.25	87.8

Table 8: Results for least-squared regression of individual parameters

To assess variations of these parameters we also performed a least-squares regression of these parameters as a function of the inverse, the inverse squared, and the square of the parameter. The results for these are shown in the following tables.

Parameter	Coefficient	Sqrt of coefficient variance [cm]	RMS [cm]	Δ RMS (reduction) [cm]	Percent of original time series data
Original			3.78		87.8
SWH (buoy)	0.0837	0.0101	3.42	0.36	80.1
SWH (laser)	0.0732	0.0084	3.36	0.52	87.8
Air Temp	-0.8463	0.1996	3.69	0.09	84.9
Sea Surface Temp	-0.7758	0.2134	3.72	0.06	83.9
Atm Pressure	678.4	539.3	3.78	0.00	84.1
Wind Speed	0.0036	0.0069	3.78	0.00	85.5
50 Hz Parameter	2.0049	0.2886	3.52	0.26	87.8

Table 9: Results for least-squared regression of inverse individual parameters

Parameter	Coefficient	Sqrt of coefficient variance [cm]	RMS [cm]	Δ RMS (reduction) [cm]	Percent of original time series data
Original			3.78		87.8
SWH (buoy)	0.0549	0.0079	3.56	0.22	80.1
SWH (laser)	0.0421	0.0059	3.50	0.28	87.8
Air Temp	-5.2949	1.2406	3.68	0.10	84.9
Sea Surface Temp	-4.5728	1.3365	3.73	0.05	83.9
Atm Pressure	3.4130	2.7394	3.78	0.00	84.1
Wind Speed	0.0001	0.0010	3.78	0.00	85.5
50 Hz Parameter	35.5755	5.3787	3.54	0.24	87.8

Table 10: Results for least-squared regression of inverse individual parameters squared

Parameter	Coefficient	Sqrt of coefficient variance [cm]	RMS [cm]	Δ RMS (reduction) [cm]	Percent of original time series data
Original			3.78		87.8
SWH (buoy)	-0.0041	0.0004	3.25	0.53	80.1
SWH (laser)	-0.0045	0.0004	3.21	0.57	87.8
Air Temp	0.0002	5e-5	3.70	0.08	84.9
Sea Surface Temp	0.0002	5e-5	3.69	0.09	83.9
Atm Pressure	-3e-7	3e-7	3.78	0.00	84.1
Wind Speed	0.0002	4e-5	3.70	0.08	85.5
50 Hz Parameter	-8e-6	1e-6	3.57	0.21	87.8

Table 11: Results for least-squared regression of individual parameters squared

In addition to the regression parameters described above, a linear least-squares regression was also tried against various combinations of these parameters including: Pressure/Temperature, Pressure x Temperature, etc.. Many combinations were attempted and they are too numerous to list all results in this paper, however none produced satisfactory results.

8.5.3. Simultaneous Regression

Since none of these parameters (inverse, inverse squared, squared, or any other combination) provided improved results over the original individual regression parameters shown in Table 8, a simultaneous regression was tried using all environmental

parameters at the same time plus what will subsequently be referred to as the inverse 50 Hz return average.

The inverse 50 Hz return average deserves some additional discussion. As stated earlier, 50 Hz data output from the laser are averaged into 1 Hz data. These 1 Hz data are then averaged over a given three-minute time interval (consisting of 181 data points) to compute the average SSH during that period. The 50 Hz return average is the average percentage of good 50 Hz laser returns for the 1 Hz data used to compute the average SSH. The 50 Hz return average is a good indicator of confidence in the laser measurement. The higher the 50 Hz return average, the greater the number of laser pulses which were read by the laser. A low 50 Hz return average is indicative of poor environmental conditions, i.e. the laser pulses are not being reflected back to the laser due to sea spray, wave cresting, foam, etc.

Although the inverse of the 50 Hz return average did not provide significant improvements in the regression analysis over the regular 50 Hz return average, it was decided to perform subsequent analysis using the inverse parameter because this term made intuitive sense as a correction factor to the laser. The linear regression coefficient derived for the inverse of the laser 50 Hz return average may be physically interpreted as correcting the laser measurement to read further away for lower values of the 50 Hz return average. This makes intuitive sense, since poor environmental conditions such as sea-spray would result in a water level measurement being closer to the laser (shorter distance).

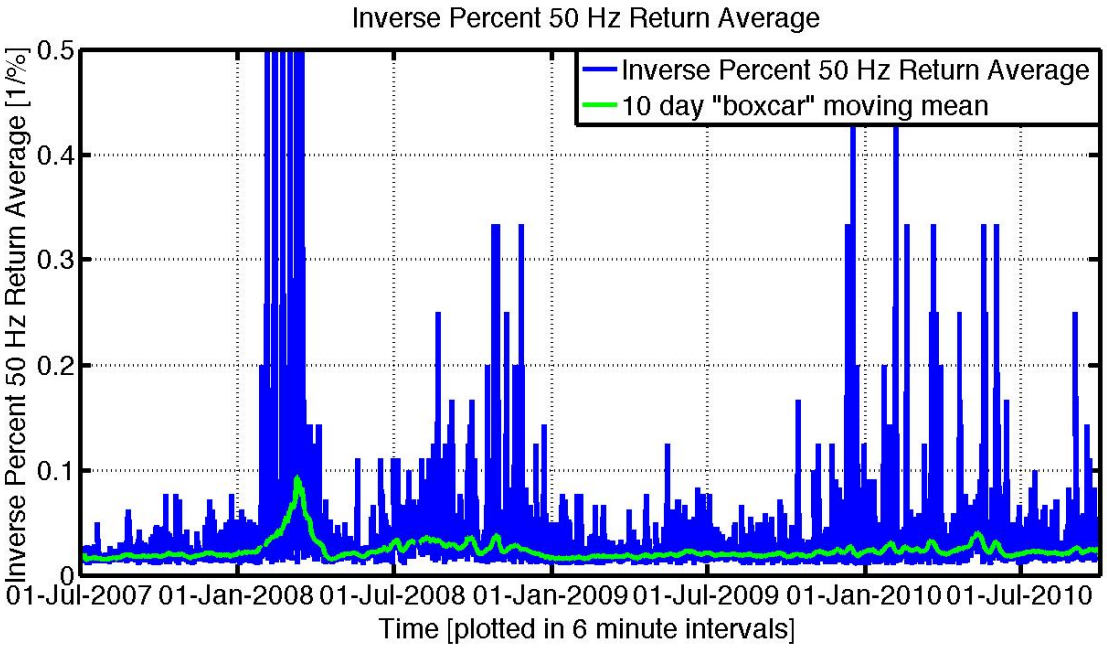

Figure 26: Inverse 50 Hz return average data from the laser over the time series.

The simultaneous regression utilized the laser derived values of SWH since this resulted in a slightly higher reduction in the resulting rms difference as well as retaining a larger percentage of the original time series due primarily to several large missing segments of data from the buoy derived SWH source. Additionally, this linear least-squares regression simultaneously provides an estimate of the vertical separation distance between the bubbler and the laser in the coefficient B_0. The regression takes the form of the equation below.

$$SSH_{Correction} = B_0 + B_1 \times \left(\frac{1}{50Hz\ average} \right) + B_2 \times (SWH) + B_3 \times (Pressure) + B_4 \times (Temp_{Air}) + B_5 \times (Temp_{SeaSurface}) + B_6 \times (Wind\ Speed) \quad \textbf{Eq. 24}$$

This regression yields the following results:

$$\hat{\mathbf{X}} = \begin{bmatrix} 27.4327 \\ 1.9587 \\ -2.6857 \times 10^{-2} \\ -4.4314 \times 10^{-4} \\ 2.8825 \times 10^{-4} \\ 1.7681 \times 10^{-3} \\ 2.0736 \times 10^{-3} \end{bmatrix}$$

$$\mathbf{P} = \begin{bmatrix} 5.6291 \times 10^{-1} & -9.0259 \times 10^{-3} & -5.3851 \times 10^{-2} & -9.9920 \times 10^{-1} \\ & 2.9698 \times 10^{-1} & 1.3330 \times 10^{-2} & -3.7087 \times 10^{-3} \\ & & 2.7899 \times 10^{-3} & 4.0660 \times 10^{-2} \\ & & & 5.4736 \times 10^{-4} \\ & & & \\ & & & \\ & & & \end{bmatrix} \text{ (columns 1 – 4)}$$

$$\mathbf{P} = \begin{bmatrix} -1.0316 \times 10^{-1} & -1.3168 \times 10^{-1} & -9.7479 \times 10^{-2} \\ 2.0344 \times 10^{-2} & -1.2583 \times 10^{-2} & 8.9778 \times 10^{-2} \\ 1.4947 \times 10^{-1} & 1.6540 \times 10^{-3} & -4.2571 \times 10^{-1} \\ 9.4051 \times 10^{-2} & 1.1540 \times 10^{-1} & 8.7299 \times 10^{-2} \\ 1.9446 \times 10^{-3} & -7.3392 \times 10^{-1} & -7.6533 \times 10^{-2} \\ & 2.0895 \times 10^{-3} & 1.9791 \times 10^{-1} \\ & & 6.9174 \times 10^{-4} \end{bmatrix} \text{ (columns 5 – 7)}$$

The above regression resulted in a reduction in the rms difference from 3.78 to 2.77 cm with 83.8% of the original time series remaining. This is a substantial reduction in the rms difference of nearly 1 cm. However, looking at the covariance matrix **P** of the above regression shows that not all of the regression parameters utilized yielded statistically significant results (assessed by comparing the square root of the variance (σ) relative to the magnitude of the particular coefficient being estimated). Thus we attempted this regression again, this time eliminating the parameters which did not yield statistically significant results. In order to place a "cut-off" to determine which

parameters should be eliminated, any parameter whose σ was of the same order of magnitude as the estimated coefficient was eliminated. This resulted in the removal of atmospheric pressure, atmospheric temperature, and sea surface temperature being eliminated. Thus the regression was run again utilizing the following equation and parameters.

$$SSH_{Correction} = B_0 + B_1 \times \left(\frac{1}{50Hz\ average} \right) + B_2 \times \left(SWH \right) + B_3 \times \left(Wind\ Speed \right) \quad \textbf{Eq. 25}$$

This regression yields the following results:

$$\hat{\mathbf{X}} = \begin{bmatrix} 27.0125 \\ 1.9473 \\ -2.7471 \times 10^{-2} \\ 1.8926 \times 10^{-3} \end{bmatrix}$$

$$\mathbf{P} = \begin{bmatrix} 8.8352 \times 10^{-3} & -7.7833 \times 10^{-1} & -3.9179 \times 10^{-1} & -2.7707 \times 10^{-1} \\ & 2.9406 \times 10^{-1} & 7.9925 \times 10^{-3} & 9.2728 \times 10^{-2} \\ & & 2.6888 \times 10^{-3} & -4.6839 \times 10^{-1} \\ & & & 6.6636 \times 10^{-4} \end{bmatrix}$$

This new regression resulted in a reduction in the rms difference from 3.78 to 2.79 cm with 85.5% of the original time series remaining. This is still a substantial reduction in the rms difference of nearly 1 cm with only a minor resulting difference from the previous regression which looked at all available parameters. Here we can see that the square root of the variances are at least an order of magnitude less than that of the estimated coefficients and more statistically relevant.

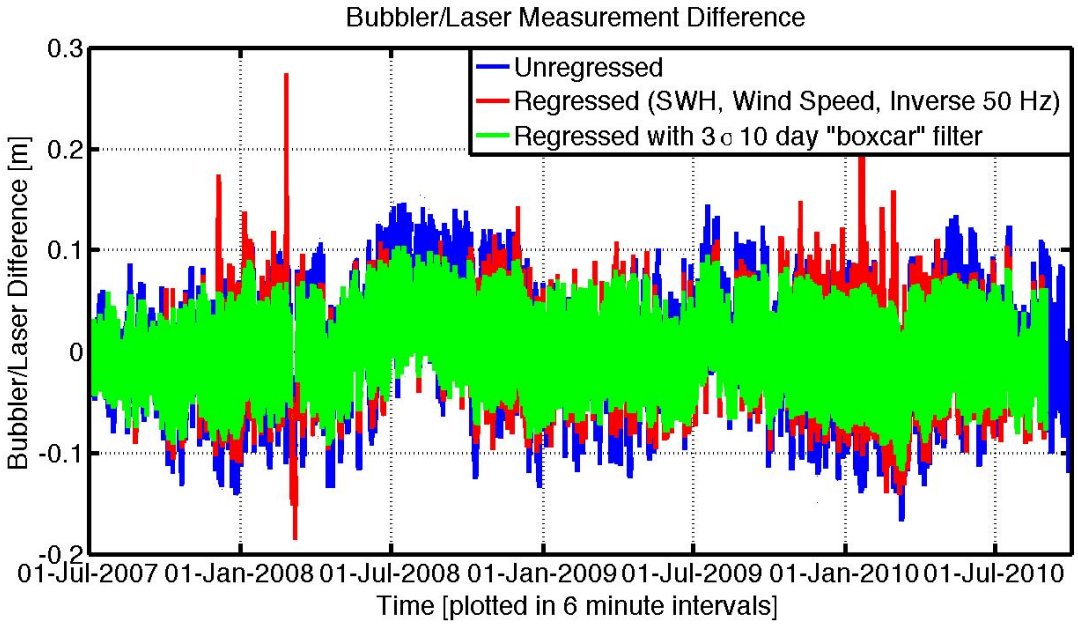

Figure 27: Comparison of linear least squares regression results

As can be seen in Figure 27 above, the regression did result in the generation of some outlier data points (red data). These are the result of individual data points being "knocked-out" due to a poor data point in either one of the regression parameter data or in the difference data. By applying an additional 3σ filter using a 10-day moving average we remove these new outliers and reduce the rms difference to 2.71 cm (green data, Figure 27). This also results in the rejection of an addition 0.7% of the original time series data, reducing the total percentage remaining from 85.5% to 84.8%. This was determined to be the best possible SSH correction based upon this least squares regression which resulted in a significant reduction in the rms difference with a minimum number of statistically significant regression parameters while maintaining the largest percentage of the original time series data. The final Bubbler/Laser measurement difference (ΔSSH) and regression parameters are shown below.

$$\Delta SSH = SSH_{Bubbler} + SSH_{Laser} - SSH_{Correction} \quad \textbf{Eq. 26}$$

$$SSH_{Correction} = B_0 + B_1 \times \left(\frac{1}{50Hz\ average} \right) + B_2 \times \left(SWH \right) + B_3 \times \left(Wind\ Speed \right) \quad \textbf{Eq. 27}$$

Where:

B_0 = 27.0125 ± 0.0088 [m] (Bubbler/Laser Vertical Separation Distance)

B_1 = -1.9473 ± 0.2941 [m] (Inverse 50Hz Average Linear correction factor)

B_2 = 0.027471 ± 0.002689 (SWH Linear correction factor)

B_3 = -0.0018926 ± 0.0006664 [sec] (Wind Speed linear correction factor)

Currently, bubbler data used in the satellite altimeter closure analysis is corrected only using SWH using an empirical correction similar to that described in Parke and Gill (1995). The current correction used by Haines et al. (2010) is:

$$SSH_{Bubbler_{Corrected}} = SSH_{Bubbler} + 0.031 \times (SWH - 1.5) \quad \textbf{Eq. 28}$$

$$\bullet For\ SWH > 1.5\ m, else\ SSH_{Bubbler_{Corrected}} = SSH_{Bubbler}$$

Thus the sea level measurement is increased as SWH increases since large waves tend to bias the bubbler measurements low. This linear correction factor of 3.1%, for SWH values greater than 1.5m, is similar to that developed in the linear least-squares regression described above and provides a good check as to the regression's validity. We

obtain similar results if we look at the unregressed Bubbler/Laser measurement difference plotted against SWH and apply a linear line fit to the data as shown in the plot below.

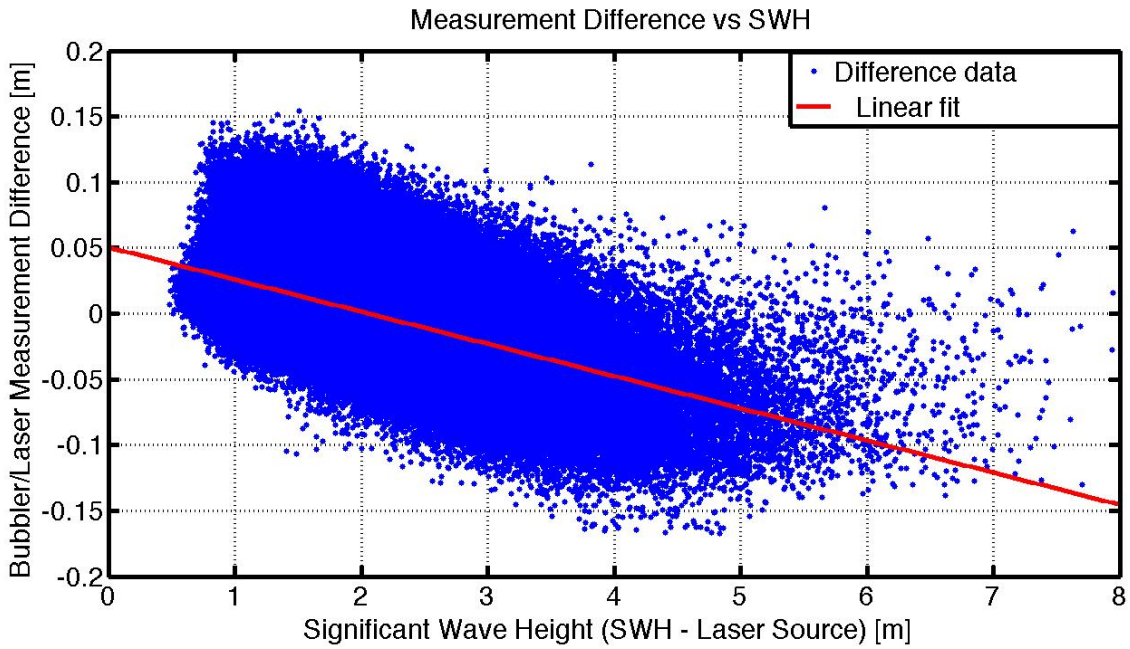

Figure 28: Unregressed Bubbler/Laser measurement difference vs SWH

Although this final regression reduces some of the systematic trends in the measurement difference time-series, as shown in Figure 27, and reduces the σ from 3.78 cm to 2.71 cm, some systematic trends are still noticeably present in the regressed data. I have been unsuccessful in finding any available parameter that completely accounts for these. There are several speculations as to why this is the case. First, many of the environmental parameters which may affect either the laser or bubbler performance are measured a considerable distance from the Harvest platform. Since sea state conditions in the open ocean can change substantially over 10 yards, much less many nautical miles, the environmental parameters used in this analysis may provide a poor representation of

actual conditions at the platform. Secondly, since the laser is enclosed in an air-tight, cast-aluminum enclosure, it is speculated that some of the remaining systematic trends may be due to temperature and pressure fluctuations inside this housing.

9. Drift Determination

One of the major reasons for placing the laser at the Harvest platform is to assess the instrument drift in the bubbler. Both digital bubblers on the Harvest platform are equipped with a Paroscientific pressure transducer, designed to minimize the loads which cause drift, and according to NOAA currently no sensor drift has been found in any of these systems. Additionally, the systems are checked and leveled as part of annual maintenance and the two sensors are compared monthly as part of NOAA's regular quality control with no noticeable drift between the two sensors (S. Gill, personal communication, February 17, 2011). However, due to the importance of monitoring the long-term drift of the altimeter SSH, it is important that the stability of the bubbler system is monitored using independent water-level measurements.

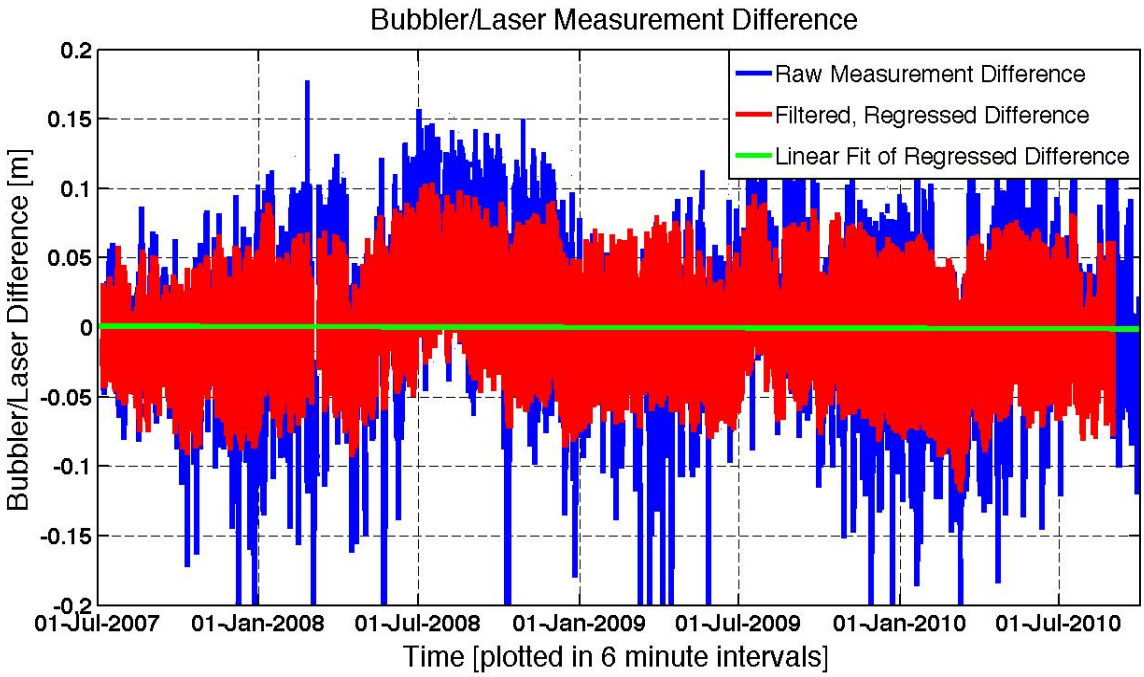

Figure 29: Plot of Raw and Regressed/Filtered Bubbler/Laser measurement difference (ΔSSH). Note that the linear fit line shows a bias drift of -0.61 mm/yr (± 2.21 mm/yr). The linear fit of the raw line is not shown for clarity but is assessed to be -1.18 mm/yr (± 2.12 mm/yr).

The drift between the two instruments was estimated using a least squares fit of a linear equation of the form y = a + b*t. Prior to the final regression detailed earlier, the drift is assessed to be -1.18 mm/yr (± 2.12 mm/yr). After performing the final regression, the drift in the bias between these two instruments is determined to be -0.61 mm/yr (± 2.21 mm/yr). Unfortunately, due to the relatively high noise levels in the data, there is a high level of uncertainty in estimated slope of the linear least squares fit and thus the drift determination is not statistically significant. A longer time-series or better regression will be necessary in order to determine this drift more accurately.

10. Instrument Corrections

Now that we have determined a correction which may be applied to the Bubbler/Laser measurement difference, we examine which parts of the correction may be separable and applied to each individual instrument. Mathematically the regression correction terms determined above are not separable and cannot be ascribed to individual behavior of the two specific instruments. A covariance analysis of the linear regression results in the following correlation coefficients between the regression parameters.

$\rho_{50Hz,WS}$ = **0.09273** (Inverse 50 -Hz correction/wind speed correlation coefficient)

$\rho_{50Hz,SWH}$ = **0.00799** (Inverse 50 -Hz correction/SWH correlation coefficient)

$\rho_{WS,SWH}$ = **-0.46839** (Wind speed/SWH correlation coefficient)

The above correlation coefficients show that there is low correlation between the inverse 50 Hz parameter and both wind speed and SWH. This is surprising since we expect the laser to be affected by these parameters and the inverse 50 Hz average is a proxy for laser performance. We believe that the filtering performed prior to the regression analysis removes any strongly correlated data segments from the analysis. We also note that there is a reasonable correlation between the wind speed and SWH.

Since the inverse 50 Hz return average is strictly a laser data derived parameter, we may safely assume that this correction may be applied to the laser only. If we also assume that this inverse 50 Hz correction term accounts for any SWH or wind speed effects on the laser, we can then separate and apply the remaining wind speed and SWH corrections directly to the bubbler measurement. This assumption seems reasonable since

the inverse 50 Hz correction has low correlation with both the wind speed and SWH and the later terms are reasonably correlated. In the following sections these terms are applied to their respective measurement device and compared to the Jason-1 and Jason-2 flyover data.

10.1. SWH vs Wind Speed

The correlation coefficient relating SWH and wind speed resulting from the regression analysis shows a reasonably large negative correlation between the two parameters. To investigate this relationship further we examine Figure 30 below which shows the mean Bubbler/Laser measurement difference over the entire time series analyzed for a given combination of SWH and wind speed.

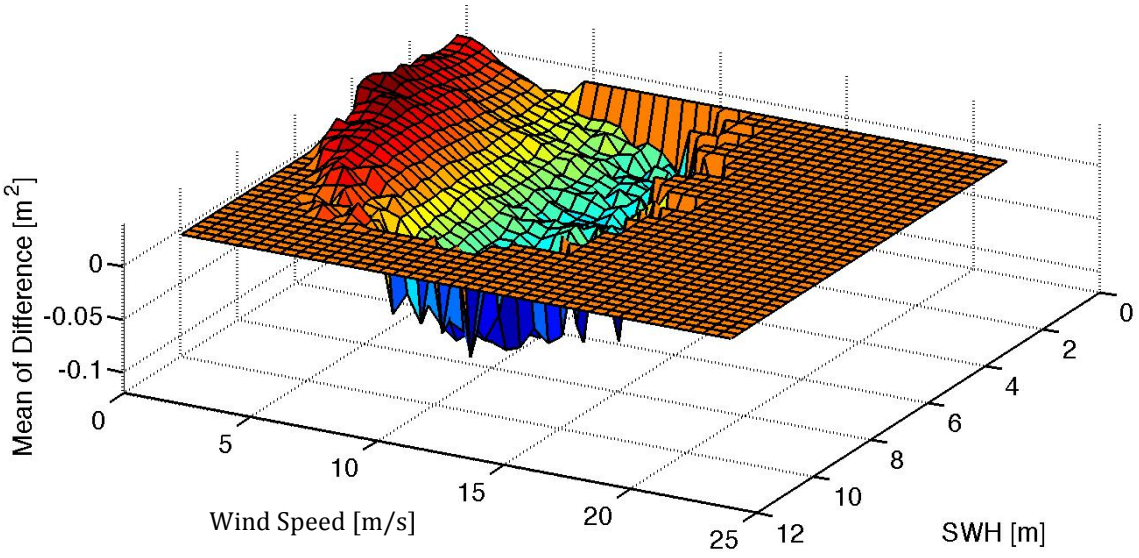

Figure 30: SWH and wind speed measurement difference.

The above plot shows an interesting relationship. At low wind speeds, regardless of the SWH, the mean measurement difference is relatively constant and positive. As the wind speed increases, this drives the measurement difference down and eventually negative. The zero point of the measurement difference is relative, however this demonstrates an interesting trend. Again, it is impossible to mathematically ascribe the wind effects on the measurement difference to one instrument or another, however we can speculate as to reasons for this phenomena. One possibility is that wind effects could cause small wind waves or even increased sea spray which could result in shorter measurements being made by the laser and thus a lower measurement difference. Another possibility could be a dynamic pressure effect causing an error in the bubbler's pressure transducer. This phenomena requires further investigation.

11. Overflight Comparison

Comparisons of the bubbler and laser SSH measurements with those from the satellite altimeter measurement systems (Jason-1 and Jason-2) at overflight times are shown in Figures 31, 32, 33, and 34. In keeping with common practice in the altimeter community, we refer to these differences as altimeter SSH biases (even though they also reflect small biases in the in-situ systems). In Figures 31 and 33, SSH measurement differences are shown between the satellite altimeter SSH and 1) the uncorrected bubbler SSH; 2) the bubbler SSH with the standard SWH correction applied (as discussed in Eq. 28); and 3) the bubbler SSH with the SWH and Wind Speed correction derived in this study (Eq. 27). In Figures 32 and 34 SSH measurement differences are shown between the satellite altimeter SSH and 1) the uncorrected laser SSH; and 2) the laser SSH with

the inverse 50-Hz return average correction derived in this study. It is important to note that absolute SSH for the laser is leveled to the bubbler and is not a meaningful indicator of improved performance.

When using the bubbler data to form the altimeter SSH biases, application of the new sea-state correction (based on SWH and wind speed), reduces the variance significantly. However, this reduction is nearly the same as that experienced using the standard (Parke and Gill, 1995; Haines et al., 2010) sea-state correction. When using the laser data to form the altimeter SSH bias estimates, we note a significant reduction in the variance in the Jason-1 SSH bias estimates using the inverse 50 Hz correction for Jason-1. The same, however, is not true for Jason-2. This result was expected since the Jason-1 overflights were plagued by periods of poor laser data and low 50 Hz return. The post-correction variances for each case are equal.

The application of this new correction to the bubbler measurement results in a change in the altimeter bias previously assessed as part of the Harvest platform calibration (Haines et al. 2010) This results in a lower average bias of 15 mm for the Jason-1 overflights and 19 mm for the Jason-2 analyzed during our time-series. This may result in increased altimeter calibration accuracy once this new bubbler correction is analyzed further.

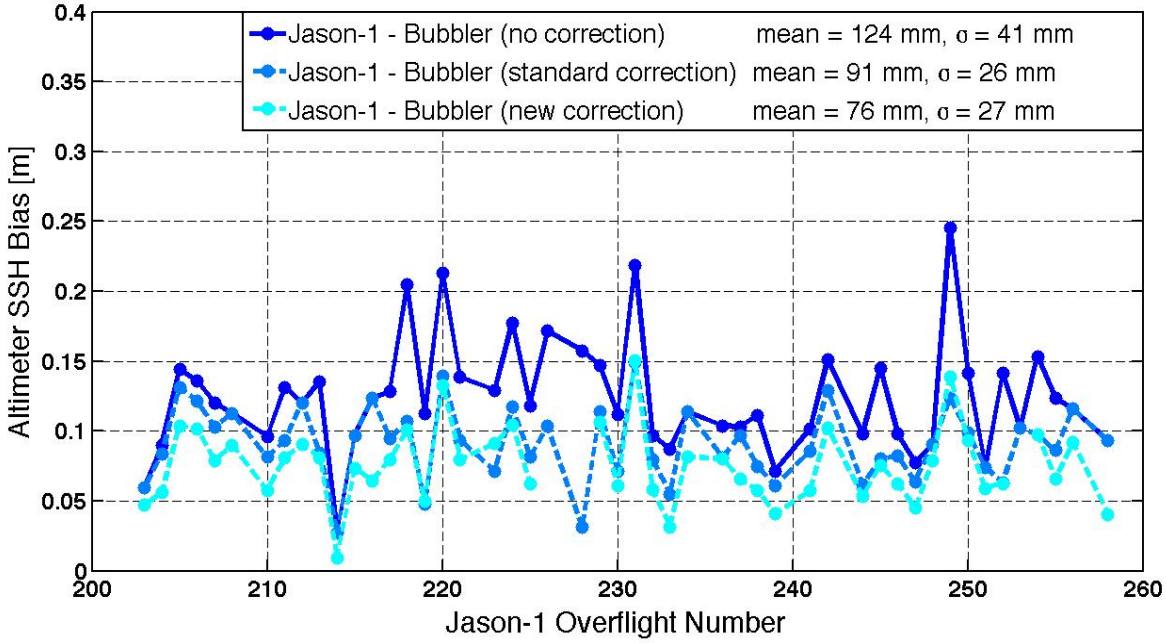

Figure 31: Plot of Jason-1 Overflight Altimeter/Bubbler SSH Bias.

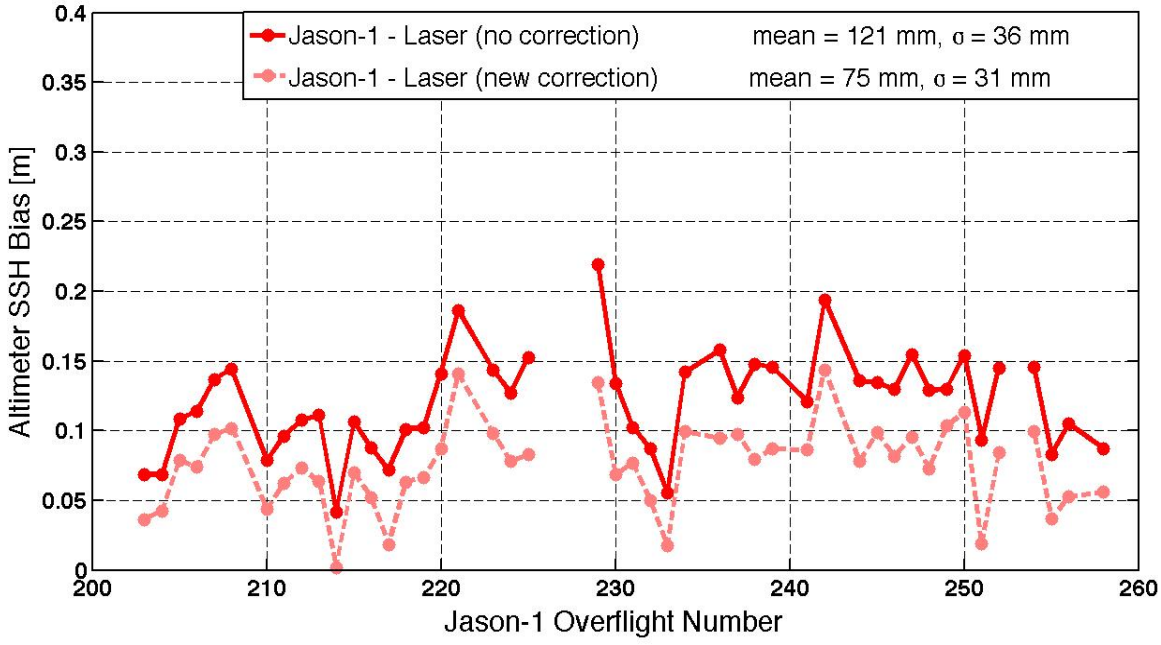

Figure 32: Plot of Jason-1 Overflight Altimeter/Laser SSH Bias. Note that that absolute SSH for the laser is leveled to the bubbler and is not a meaningful indicator of performance.

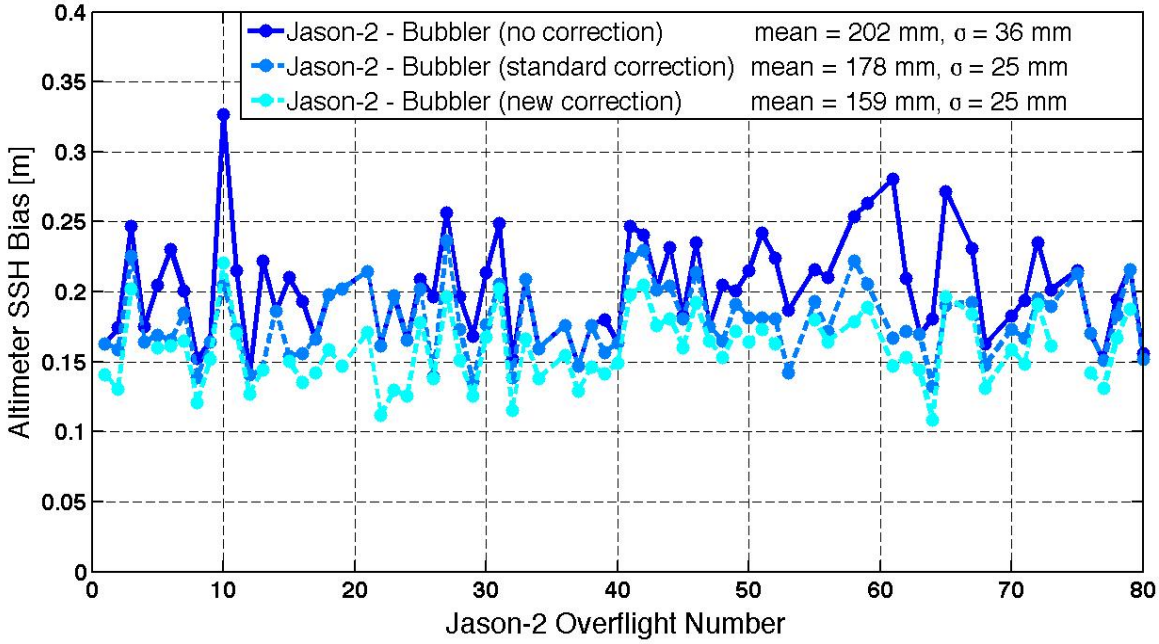

Figure 33: Plot of Jason-1 Overflight Altimeter/Bubbler SSH Bias.

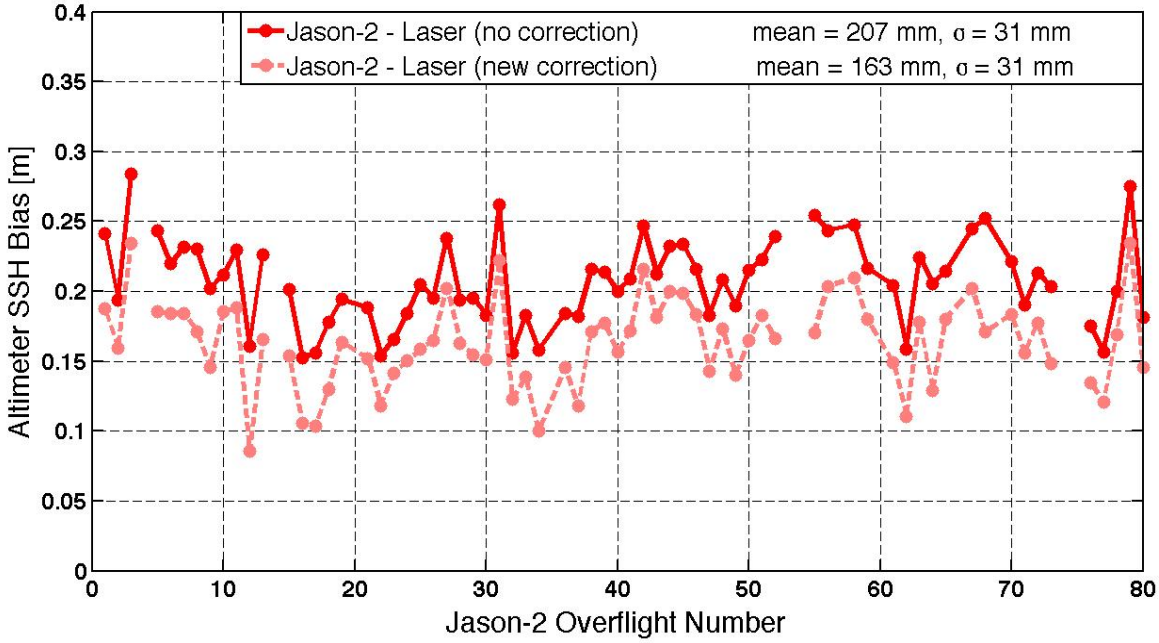

Figure 34: Plot of Jason-2 Overflight Altimeter/Laser SSH Bias. Note that that absolute SSH for the laser is leveled to the bubbler and is not a meaningful indicator of performance.

It is also important to note that there are segments of missing flyover data in the above figures. For the case of the bubbler or laser data, this could be due to missing data or data which was filtered out as being of poor quality based on the previous filtering discussion. In the case of the satellite altimeter data this could also be due to missing data (which in the above figures only occurs for Jason-1 Flyover 243) or data which was deemed of poor quality and filtered out. For the satellite altimeter data, filtering is performed using a threshold of the measured "backscatter" for a given overflight. This backscatter parameter can be considered a proxy for the quality of the altimeter data and the threshold is separately determined for each satellite. Periods of high backscatter are known as σ^0 blooms (Mitchum, 2004). For Jason-1 these occur for overflights 209, 222, 227, 235, 240, 257, and 259 during the time period analyzed. For Jason-2 these occur for overflights 20, 35, 54, 57, 60, 66, 69, and 74 during the time period analyzed.

12. Summary

Despite significant challenges, the LIDAR system has shown promise in being able to assess drift in the bubbler as well as the dependencies on SWH and wind speed. In addition, it provides an additional estimate of SWH at the platform, which may be used for more accurate analysis since it is collocated with the bubbler. More data, however, are needed in order to make an assessment of these parameters with the desired accuracy (e.g., drift to better than 1 mm/yr). Once these dependencies are better understood, the LIDAR system may prove an eventual successor to the traditional submerged tide gauges.

There are still some remaining systematic trends in the difference between the bubbler and laser measurements which we have been unable to remove or account for. Since many of the environmental parameters which may affect either the laser or bubbler performance are measured a considerable distance from the Harvest platform, the environmental parameters used in this analysis may provide a poor representation of actual conditions at the platform. Additionally, since the laser is enclosed in an air-tight, cast-aluminum enclosure, it is speculated that some of the remaining systematic trends may be due to temperature and pressure fluctuations inside this housing. Future visits to the platform by the University of Colorado will hopefully allow the installation of environmental monitoring equipment to provide data such as wind speed, wind direction, temperature, and pressure directly at the platform site. These should also include the installation of thermocouples and a pressure transducer inside the laser housing to identify potential influences, if any, on the laser measurement. Additionally an accurate survey of the laser is necessary to exactly determine the vertical separation distance between the laser and bubbler.

Finally, environmental conditions at the Harvest platform are harsh and as such make in-situ characterization of the laser performance difficult. Future work utilizing techniques such as the Van de Casteele test (Miguez et al., 2008) may yield better performance characterization under different operating conditions. Additional controlled testing to attempt to quantitatively determine laser performance dependence on laser settings and environmental factors would further successful comparison between the bubbler and laser measurement devices.

References

Bonnefond, P., P. Exertier, O. Laurain, Y. Me´nard, A. Orsoni, G. Jan, and E. Jeansou. 2003. Absolute calibration of Jason-1 and TOPEX/Poseidon in Corsica. *Mar. Geod.* 26(3–4):261–284.

Bonnefond, P., P. Exertier, O. Laurain, G. Gwenaele. 2010. Absolute Calibration of Jason-1 and Jason-2 Altimeters in Corsica during the Formation Flying Phase. *Mar. Geod.* 33(Sup. 1):80–90.

Chelton, D. B., J. C. Ries, B. J. Haines, L.–L. Fu, and P. S. Callahan. 2001. Satellite altimetry. Chapter 1 in *Satellite altimetry and earth sciences: A handbook of techniques and applications*. San Diego, CA: Academic Press.

Christensen, E. J., B. J. Haines, S. J. Keihm, C. S. Morris, R. S. Norman, G. H. Purcell, B. G. Willams, B. C. Wilson, G. H. Born, M. E. Parke, S. K. Gill, C. K. Shum, B. D. Tapley, R. Kolienkiewicz, and R. S. Nerem. 1994. Calibration of TOPEX/Poseidon at platform Harvest. *J. Geophys. Res.* 99(C12):24465–24485.

Gill, S. K., and M. E. Parke. 1995. Platform Harvest sea level measurement comparisons. *Mar. Geod.* 18(1–2):85–96.

Gill, S. K., R. F. Edwing, D. F. Jones, T. N. Mero, M. K. Moss, M. Samant, H. H. Shih, and W. M. Stoney. 1995. NOAA/National Ocean Service Platform Harvest instrumentation. *Mar. Geod.* 18(1–2):49–68.

Haines, B. J., E. J. Christensen, R. A. Norman, M. E. Parke, G. H. Born, and S. K. Gill. 1996. Altimeter calibration and geophysical monitoring from collocated measurements at the Harvest oil platform. *EOS* 77(22). Fall Meet. Suppl:W16.

Haines, B., D. Dong, G. Born, and S. Gill. 2003. The Harvest experiment: Monitoring Jason-1 and TOPEX/POSEIDON from a California offshore platform. *Mar. Geod.* 26(3–4):239–259.

Haines, B., G. Born, S. Desai, and S. Gill. 2004. Monitoring Jason-1 and TOPEX/POSEIDON from an offshore platform: Latest results from the Harvest experiment. Proceedings of the Ocean Surface Topography Science Team, November 4–6, in St. Petersburg, Florida.

Haines, B., S. Desai, and G. Born. 2010. The Harvest Experiment: Calibration of the Climate Data Record from TOPEX/POSEIDON, Jason-1, and the Ocean Surface Topography Mission. *Mar. Geod.* 33(Sup. 1):91–113.

International Oceanographic Commission (IOC). February 2002. Manual on Sea Level Measurement and Interpretation: Volume III - Reappraisals and Recommendations as of the year 2000.

International Oceanographic Commission (IOC). 2006. Manual on Sea Level Measurement and Interpretation: Volume IV – An Update to 2006.

Kinsman, B. 1965 Wind Waves: Their Generation and Propagation on the Ocean Surface. Englewood Cliffs, N.J.: Prentice Hall.

Lomb, N.R. 1976. Least-squares Frequency Analysis of Unequally Spaced Data. *Astrophysics And Space Science*. 39: 447-462.

Martinez-Benjamin, J. J., Martinez-Garcia, M., Gonzalez Lopez, S., Nunez Andres, A. Buill Pozuela, F., Espino Infantes, M., Martin Davila, J., Garate Pasquin, J., Garcia Silva, C., Bonnefond, P., Laurain, O., Baron Isanta, A. M., Ortiz Castellon, M. A., and Talaya Lopez, J. 2004. Ibiza Absolute Calibration Experiment: Survey and Preliminary Results. *Mar. Geod.* 27(3–4):657–681.

Miguez, B. M., Testut, L., Wöppelmann, G. 2008. The Van de Casteele Test Revisited: An Efficient Approach to Tide Gauge Error Characterization. *J. Atmos. Ocean. Tech*., 25: 1238–1244.

Mitchum, G. 1998. Monitoring the stability of satellite altimeters with tide gauges. *J. Atmos. Ocean. Tech.* 15:721–730.

Mitchum, G., D. W. Hancock III, G. S. Hayne, AND D. C. Vandemark. 2004. Blooms of σ^0 in the TOPEX Radar Altimeter Data. *J. Atmos. Ocean. Tech.* 21:1232–1245.

Morris, C. S., S. J. Dinardo, and E. J. Christensen. 1995. Overview of the TOPEX/Poseidon platform Harvest verification experiment. *Mar. Geod.* 18(1–2):25–38.

National Oceanic and Atmospheric Administration (NOAA). April 2010. Air Gap Field Installation Guide, Version 2.0.

Parke, M. E., and Gill, S. K. 1995. On the sea-state dependence of sea level measurements at Platform Harvest. *Mar. Geod.* 18(1–2):105–116.

Parke, M. E., and Walsh, E. J. 1995. Altimeter Footprint Dimensions. *Mar. Geod.* 18(1–2):129–137.

Parke, M. E., and C. S. Morris. 1995. Significant wave height comparisons between TOPEX and Platform Harvest. *Mar. Geod.* 18(1–2):97–104.

Pavlis, E. C., Stelios, P. M., and the GAVDOS Team. 2004. The GAVDOS Mean Sea Level and Altimeter Calibration Facility: Results for Jason-1. *Mar. Geod.* 27(3–4):631–655.

Press, W. H., Teukolsky, S. A., Vetterling, W. T., Flannery, B. P., 2007. Numerical Recipes 3rd Edition: The Art of Scientific Computing. New York: Cambridge University Press.

Scargle, J. D. 1982. Studies in Astronomical Time Series Analysis. II. Staticstical Aspects of Spectral Analysis of Unevenly Spaced Data. *The Astrophysical Journal*. 263:835-853.

Shum, C., Yi, Y., Cheng, K., Kuo, C., Braun, A., Calmant, S., Chambers, D. 2003. Calibration of JASON-1 Altimeter over Lake Erie. *Mar. Geod.* 26:335–354.

Watson, C., Coleman, R., White, N., Church, J., Govind, R., 2003. Absolute Calibration of TOPEX/Poseidon and Jason-1 Using GPS Buoys in Bass Strait, Australia. *Mar. Geod.* 26:285–304.